



Институт за нуклеарне науке „Винча“
Универзитет у Београду

VINČA Institute of Nuclear Sciences
University of Belgrade

2019

Controllable Synthesis of Fe₃O₄-Wollastonite Adsorbents for Efficient Heavy Metal Ions/Oxyanions Removal

Rusmirović, Jelena D.; Obradović, Nina; Perendija, Jovana; Umićević, Ana; Kapidžić, Ana; Vlahović, Branislav; Pavlović, Vera; Marinković, Aleksandar D.; Pavlović, Vladimir B.

Published in:

Environmental Science and Pollution Research

DOI:

[10.1007/s11356-019-04625-0](https://doi.org/10.1007/s11356-019-04625-0)

Document version:

Final peer-reviewed version (often known as postprint)

Recommended citation:

Rusmirović, J. D., Obradović, N., Perendija, J., Umićević, A., Kapidžić, A., Vlahović, B., ... & Pavlović, V. B. (2019). Controllable synthesis of Fe₃O₄-wollastonite adsorbents for efficient heavy metal ions/oxyanions removal. *Environmental Science and Pollution Research*, 1-20.

This work is licensed under [Creative Commons Attribution-Noncommercial-NoDerivates 4.0 International Licence](https://creativecommons.org/licenses/by-nc-nd/4.0/)



[Click here to view linked References](#)

Controllable Synthesis of Fe₃O₄-Wollastonite Adsorbents for Efficient Heavy Metal Ions/Oxyanions Removal

Jelena D. Rusmirović^{1*}, Nina Obradović², Jovana Perendija³, Ana Umičević⁴, Ana Kapidžić⁴, Branislav Vlahović⁵, Vera Pavlović⁶, Aleksandar D. Marinković⁷, Vladimir B. Pavlović^{2,8}

¹*Innovation Center of the Faculty of Technology and Metallurgy, University of Belgrade, Karnegijeva 4, 11120 Belgrade, Serbia, jrusmirovic@tmf.bg.ac.rs*

²*Institute of Technical Sciences of SASA, Knez Mihailova 35/IV, 11000 Belgrade, Serbia*

³*Institute of Chemistry, Technology and Metallurgy, University of Belgrade, Njegoševa 4, 11000, Serbia*

⁴*Vinča Institute of Nuclear Sciences, University of Belgrade, Serbia*

⁵*North Carolina Central University, Department of Mathematics and Physics, Durham, United States*

⁶*Faculty of Mechanical Engineering, Kraljice Marije 16, 11120 Belgrade, Serbia*

⁷*Faculty of Technology and Metallurgy, University of Belgrade, Karnegijeva 4, 11120 Belgrade, Serbia*

⁸*Faculty of Agriculture, University of Belgrade, Nemanjina 6, 11080 Belgrade-Zemun, Serbia*

***Corresponding author:** Jelena Rusmirović, Innovation Center of the Faculty of Technology and Metallurgy, University of Belgrade, Karnegijeva 4, 11120 Belgrade, Serbia, jrusmirovic@tmf.bg.ac.rs

Abstract

Iron oxide, in the form of magnetite (MG), functionalized porous wollastonite (WL) was used as an adsorbent for heavy metal ions (cadmium and nickel) and oxyanions (chromate and phosphate) removal from water. The porous WL was synthesized from calcium carbonate and siloxane by controlled sintering process using low molecular weight submicro-sized poly(methyl methacrylate) as a pore-forming agent. The precipitation of MG nanoparticles was carried out directly by a polyol-medium solvothermal method or *via* branched amino/carboxylic acid cross-linker by solvent/nonsolvent method producing WL/MG and WL-γ-APS/MG adsorbents, respectively. The structure/properties of MG functionalized WL was confirmed by applying FTIR, Raman, XRD, Mössbauer, and SEM analysis. Higher adsorption capacities of 73.126, 66.144, 64.168 and 63.456 mg g⁻¹ for WL-γ-APS/MG in relation to WL/MG: 55.450, 52.019, 48.132 and 47.382 mg g⁻¹ for Cd²⁺, Ni²⁺, phosphate and chromate, respectively, were obtained using non-linear Langmuir model fitting. Adsorption phenomena were analyzed using monolayer statistical physics model for single adsorption with one energy. Kinetic study showed exceptionally higher pseudo second-order rate constants for WL-γ-APS/MG, e.g. 1.17 – 13.4 times, with respect to WL/MG indicating importance of both WL surface modification and controllable precipitation of MG on WL-γ-APS.

Keywords Calcium metasilicates ceramic; Magnetite functionalization; Solvent/nonsolvent method; Polyol-thermal method; Heavy metals; Adsorption; Fe₃O₄.

Introduction

Rapid global industrialization increases the amount of effluent consisted of chemical wastes such as volatile organic compounds (industrial solvents), heavy metals and oxyions, pharmaceutical drugs and their metabolites, *etc.* Industrial effluents are one of the prime sources of environmental toxicity that deteriorates water quality (Paul 2017). Long-term exposure to heavy metals, such as cadmium, nickel and chromium (Cd^{2+} , Ni^{2+} and Cr(VI)), by ingestion/inhalation leads to a buildup in kidneys and possible kidney disease, lung damage, cancer, and fragile bones (Karthikeyan et al. 2005; Martin and Griswold 2009). Due to that, Environmental Protection Agency (EPA) limits concentration of Cd^{2+} to 0.005 ppm and of Ni^{2+} and Cr(VI) to 0.1 ppm in water (EPA 2014). As an essential nutrient required for critical biological reactions maintaining the normal homeostatic control of the cell, and growth of algae phosphorus is an important component of different cellular structures (Mezenner and Bensmaili 2009; Razzaque 2011). The phosphorus concentration has to be limited in order to control algal blooming (Mezenner and Bensmaili 2009). The phosphate discharge standard of wastewater is averaged on 1–2 ppm in order to satisfy the stringent EPAs limit of phosphorous concentration in natural water (0.02 ppm) (Rout et al. 2015, 2016). With the aim to maintain the pollutant concentration within the permissible limits, purification/pollutant removal from industrial water becomes imposed as a solution for susceptibility environmental toxicity.

In recent years, a great attention was directed in development of physically and chemically removing of heavy metals from contaminated water by a variety of methods, including membrane separation, flocculation, adsorption, ion-exchange, precipitation, evaporation, and electrolysis (D'Halluin et al. 2017; Iannazzo et al. 2017; Han et al. 2018). Due to low operational cost and high efficient in the removal of many heavy metal ions, as well as possibility of using natural materials as adsorbents, the adsorption stands out as one of the most efficient and widely used techniques for removing of metal ions (Zeng et al. 2015). Development of the more effective and cheaper adsorbents, that may be of mineral, organic or biological origin has been studied in the recent decade (Abdel-Halim and Al-Deyab 2011; Zeng et al. 2015). Calcium silicates have received considerable attention as adsorbent for heavy metal adsorption due to their excellent bioactivity and biocompatibility (Chen et al. 2008; Zhao et al. 2014). Wollastonite (WL) is a naturally occurring and cheap α -calcium metasilicate ($\alpha\text{-CaSiO}_3$) that is commonly used in preparing ceramic bodies and other materials, but lately have used as an adsorbent in water pollution control (Sharma et al. 1990b, a, 2007; Sharma 2001; Obradović et al. 2017a). Calcium oxide (CaO) and silicon dioxide (SiO_2) are the main constituents of WL ($\text{CaO/SiO}_2=48.18\%/48.52\%$ by weight) that can be responsible for heavy metals adsorption (Sharma 2001). Sharma et al. were investigated ability of natural WL to remove Cd^{2+} , Ni^{2+} and Cr(VI) ions from water and found maximum removal of 93.6% and 69.5% for Cd^{2+} and Cr(VI) ions, respectively, and maximum adsorption capacity of 6.52 mg g^{-1} for Ni^{2+} ions (Sharma et al. 1990b, a, 2007). The main disadvantage of WL for use as an adsorbent for the removal of pollutants from aquatic systems is the hydrophilicity of its surface. Surface modification, as a key process in functional WL preparation, renders hydrophilic WL surface hydrophobic (Ding et al. 2011). In order to reduce the hydrophilicity of the WL surface and, therefore, increase the heavy metals ions adsorption capacity, it is necessary to functionalize its surface.

Iron oxides and oxidehydroxides based adsorbents have been widely used in water treatment systems for the removal of ionic pollutants (Markovski et al. 2014b, a, Taleb et al. 2015, 2016a; Lin et al. 2017; Zeng et al. 2017). Due to expressed electrostatic attraction and ligand exchange with heavy metal ions, magnetite (MG – Fe_3O_4) nanoparticles were shown to be highly efficient materials for heavy metal ion removal by adsorption (Kalantari et al. 2014). Besides, using of MG in production hybrid adsorbents resolve separation problems because, due to their magnetic property, MG particles can be easily separated from aqueous solutions using an external magnetic field (Kalantari et al. 2014). Moreover, amination of MG surface helps in formation of uniform Fe_3O_4 deposit without appreciable nanoparticle aggregation. In that way, improvement of two benefit was achieved: controllable MG precipitation due to the strong metal chelation of amine groups and improved adsorption performances of the obtained adsorbent (Qi et al. 2017). To the best of our knowledge, there are no examples in the literature dealing with the removal of Cd^{2+} , Ni^{2+} , chromate and phosphate ions by WL based adsorbent with impregnated MG particles.

Besides the adsorbent morphology and surface properties, the operating conditions play an important role in achieved high adsorption capacities. Many theoretic studies (isothermal, kinetic, statistical-physic models) are carried out to understand the behavior of single-compound adsorption systems since the operating conditions can be potentially infinite in terms of combination of pollutant concentration, temperature and time of the pollutant/adsorbent contact (Sellaoui et al. 2016a, b, 2017a, b). Freundlich and Langmuir models are mostly used to analyze the adsorption equilibrium of heavy metal removal using WL or MG based adsorbents in a single component system (Sharma et al. 1990b, a, 2007; Taleb et al. 2016b; Obradović et al. 2017b, a). More precise interpretation of single adsorption isotherms can be obtained using statistical physic theory, etc. monolayer models with one or two energies. The obtained theoretical results connect experimental result with successfulness of the applied adsorbent synthesis process and operation conditions.

In the present work, the ability of a hybrid material consisting of the WL as a support of MG particles, for removal of Cd^{2+} , Ni^{2+} , chromate and phosphate ions from aqueous solutions was studied. The ions adsorption capacity of the WL impregnated with MG can be controlled either by directly precipitation of MG particles or polyol-medium solvothermal method and *via* (3-aminopropyl)trimethoxy-silane cross-linker by solvent/nonsolvent system method. The adsorption experiments were performed in order to analyze the influence of the MG precipitation method, adsorbent amount, adsorption temperature and contact time on achieved capacities. Moreover, the present work is a modeling study of heavy metals ion/oxyanions removal and provides useful information about the adsorption mechanisms in single-compound system.

Experimental section

Materials

All reagents were of analytical grade and used without purification. Deionized water (DW), of resistivity of $18\text{ M}\Omega\text{cm}$, was used. Ultra-pure HNO_3 acid and diethylene-triaminepentaacetic acid (DETAPAA) were supplied from Fluka. Iron(III) chloride hexahydrate ($\text{FeCl}_3 \cdot 6\text{H}_2\text{O}$), iron(II) sulphate heptahydrate ($\text{FeSO}_4 \cdot 7\text{H}_2\text{O}$), sodium hydrogen carbonate (NaHCO_3), sodium acetate (NaAc), polyethylene glycol 6000 (PEG-6000), (3-aminopropyl)triethoxysilane,

methanol, methyl methacrylate (MMA), potassium persulphate, calcium carbonate (CaCO_3), *N,N*-dimethylformamide (DMF), toluene and isopropyl alcohol were supplied from Sigma-Aldrich. Methylhydro-cyclosiloxane was supplied from abcr GmbH. Standard solutions of nickel(II) nitrate hexahydrate (1000 ppm) was supplied from Accustandard. Cadmium(II) nitrate tetrahydrate (1000 ppm) was supplied from Panreac. Chromium(VI) standard for ICP (1000 ppm) was supplied from Sigma-Aldrich. Phosphate standard solution (1000 pm) was supplied from Merck KGaA.

Synthesis of submicropoly(methyl methacrylate) spheres

Synthesis of submicro poly(methyl methacrylate) spheres (PMMA) was done according to the procedure described elsewhere (Shim et al. 2004). Polymerization was carried out in a 250 ml three-necked glass reactor equipped with a magnetic stirrer (stirring rate 100 rpm), reflux condenser, nitrogen inlet tube and an oil bath. Mixture of 100 ml of methanol and 50 ml water was added in the glass reactor and followed by addition of 5 g of MMA and the temperature was raised up to 70 °C. Thereafter, the aqueous potassium persulphate (KPS) solution (0.0375 g of KPS in 10 ml of water) was added and the polymerization was initiated under nitrogen (inert) atmosphere at 70 °C. After 1 h, the mixture was cooled down using an ice-bath and PMMA was washed three times with a cold methanol/water mixture (90/10 v/v) by applying repeated centrifugation/ultrasound treatment.

Synthesis of diethylenetriaminepentaacetic acid dianhydride

Synthesis of diethylenetriaminepentaacetic acid dianhydride (DETAPADA) was done according to the procedure described elsewhere (Capretta et al. 1995). In a dry three-necked glass reactor equipped with a magnetic stirrer, reflux condenser, nitrogen inlet tube and calcium chloride protection tube, immersed in an oil bath, 23.6 g of DETAPAA (60.0 mmol) was suspended in 31 ml of dry pyridine followed by addition of 24 ml of acetic anhydride. The mixture was heated at 65 °C for 24 h under intensive mixing, cooled down and filtered under vacuum and inert atmosphere. The obtained product, white solid, was collected and washed with 200 ml of acetic anhydride and 200 ml of diethyl ether and dried under vacuum at 50 °C for 6 h.

Synthesis of wollastonite based adsorbent

Wollastonite-based adsorbents were synthesized in a two-step pressureless sintering process described in the previous research (Obradović et al. 2017a). In the first step 7.79 g methylhydro-cyclosiloxane was dissolved in 100 ml of isopropyl alcohol under magnetic stirring at ambient temperature. Thereafter, 9.00 g of micro-sized CaCO_3 was added and mixed for 10 min, followed by ultrasound treatment (*Bandelin electronic ultrasonic bath, Berlin, Germany, power 120 W, frequency 35 kHz*) for 20 min and dried overnight at 80 °C. The obtained paste was calcined in a furnace at 250 °C during 30 min, with a 5 °C/min heating rate. In the second step, the as-prepared wollastonite powder (0.80 g) was carefully homogenized with a pore-forming agent (0.20 g submicro PMMA spheres), molded in a cylinder pallet (dimension 5 mm· ϕ 10) and sintered at 900 °C during 1 h, with a 5 °C/min heating rate.

Direct attaching of MG spheres on wollastonite

The generation of MG nanoparticles was carried out by a polyol-medium solvothermal method according to the literature description (Wang et al. 2011). In single necked glass reactor of 50 ml, 0.405 g of $\text{FeCl}_3 \cdot 6\text{H}_2\text{O}$ was dissolved into 20 ml ethylene glycol, producing an orange solution. 1.0 g of sintered wollastonite was homogeneously dispersed applying sonication for 3 h. Addition of NaAc (1.8 g) and PEG-6000 (0.5 g), keeping a constant mechanical stirring at 800

rpm for 30 min, provided pH and viscosity adjustment of the dispersion. The obtained viscous product was transferred in a Teflon-lined stainless steel autoclave of a 80 ml capacity followed by heating at 200 °C for 8 h. The black precipitates, obtained after cooling the reaction mixture, were washed with water and ethanol three times and dried in a vacuum oven at 60 °C. The final product was labeled WL/MG.

Attachment of MG nanoparticles on branched carboxyl functionalized wollastonite

Stepwise synthesis of amino-functionalized and subsequently carboxy terminal functionalization of WL was performed by applying the modified literature method (Taleb et al. 2015). Amino group functionalization of WL was achieved by a direct silanization of WL with (3-aminopropyl)triethoxysilane (γ -APS). The product was named WL- γ -APS. In a three-necked glass reactor of 100 ml, equipped with a magnetic stirrer, reflux condenser, nitrogen inlet tube and an oil bath for heating, 1.0 g of WL was dispersed into 50 ml of toluene under continuous stirring, then 1.0 ml of triethylamine and 1.0 ml of γ -APS were added into the suspension, and followed by refluxing at 80 °C for 12 h under a nitrogen atmosphere. WL- γ -APS was purified by washing in ethanol, dried under vacuum at 60 °C and then used for carboxylic acid modification in order to obtain more reactive centers for MG precipitation. The quantitative Kaiser test (Sarin et al. 1981) predicted the concentration of terminal amino functions present on the WL- γ -APS material to be 2.50 mmol g⁻¹. Modified WL- γ -APS (1.2 g) was dispersed in 10 ml of DMF under stirring, and after 10 ml of 0.1 mol l⁻¹ solution of DETAPADA was added into the suspension, and mixed at room temperature for 24 hrs. Finally, the product (WL/DA) was dried under vacuum at 60 °C and used for attaching of MG spheres according to the procedure described elsewhere in the literature (Taleb et al. 2015). The acidic site concentrations were determined using the Boehm titration method (Boehm 1994), and the determined acid value for WL/DA was found to be 4.3 mmol g⁻¹.

In the last step, WL/DA (1.3 g) was sonicated in 30 ml of toluene with simultaneous introduction of nitrogen for 30 min, and after pH of dispersion was adjusted at ~6. The reaction was continued by drop-wise addition of 1.0 ml of 0.125 mol l⁻¹ FeSO₄·7H₂O solution for 15 min under magnetic stirring and inert atmosphere. Neutralization of the reaction mixture with a 1 mol l⁻¹ NaHCO₃ buffer solution cause precipitation of iron oxide in the MG form. The reaction took place by heating at 90 °C for 48 h while a black product was obtained. The obtained product was filtered, washed with 200 ml DW and dried applying vacuum/drying treatment at 60 °C/2000 Pa for 6 hours. The final product was named WL- γ -APS/MG. Schematic illustration of WL modification methods is shown in Fig. 1.

Fig. 1.

Adsorption and kinetic experiments

Batch adsorption experiments of Cd²⁺, Ni²⁺, Cr(VI) and phosphate ions removal, under mixing using a laboratory shaker (*Digital Heating Shaking Drybath* by Thermo SCIENTIFIC), were applied to determine adsorption capacities and investigate effects of diffusional processes on the performance of synthesized adsorbents. An appropriate adsorbent mass ($m = 1.0, 1.5, 2.5, 5.0, 7.5$ and 10 mg), was placed in glass vials containing 10 ml of the standard solutions of ions of interest (Cd²⁺, Ni²⁺, Cr(VI) and phosphate ions) at initial concentrations, C_i , of 10 ppm.

According to the determined values of the point of zero charge of the WL based adsorbents and the ion distribution, the pH values of the solutions of Cd²⁺ and Ni²⁺ ions were set at 7.5 and for the solutions of Cr(VI) and phosphate ions were set at 6.5. The adsorption and kinetic experiments were performed at 298, 308 and 318 K. The adsorption kinetic was studied by varying the adsorbent/ion contact time in the range 5-90 min at C_i=10 ppm. The adsorption capacities of Cd²⁺, Ni²⁺, Cr(VI) and phosphate ions removal using WL based adsorbents were calculated according to the following Eq. (1):

$$q = \left((C_i - C_f) / m \right) V \quad (1)$$

Where q is the adsorption capacity in mg g⁻¹, C_i and C_f are the initial and final concentrations of ions in ppm, V is the volume of solution in l, and m is the mass of the adsorbent in g. After adsorption experiments, WL/MG and WL- γ -APS/MG adsorbents were washed with DW. Further, in order to evaluate the adsorbent regeneration capabilities, wet adsorbents were redispersed in 20 ml of solution for regeneration (NaOH/NaCl, 0.5/0.5 mol l⁻¹) (Taleb et al. 2016b). The amount of desorbed ions in effluent water was measured after mixing by the laboratory shaker for 3 h in a batch system. Three consecutive adsorption/desorption cycles were performed.

Characterization method

Fourier transforms infrared spectroscopy (FTIR) spectra of the WL based adsorbents were recorded in the absorbance mode using a Nicolet™ iS™10 FT-IR Spectrometer (Thermo Fisher SCIENTIFIC) with Smart iTR™ Attenuated Total Reflectance (ATR) Sampling accessories, within the range of 400-4000 cm⁻¹, at a resolution of 4 cm⁻¹ and in 32 scan mode.

The X-ray powder diffraction patterns were obtained using a Philips PW-1050 diffractometer with λ Cu-K α radiation and a step/time scan mode of 0.05 ° s⁻¹. The measurements were taken at room temperature in air.

The morphology of the sintered powders was characterized by the scanning electron microscopy (JEOL JSM-6390 LV). The pellets were crushed and covered with gold in order to perform these measurements.

Raman spectra of the WL-based adsorbent, recorded in the range 200–1200 cm⁻¹, were collected with a Horiba JobinYvon Aramis Raman/PL System. The system employed a 633 nm laser (output power 4 mW, on sample 1 mW). All the measurements were realized using a spectrometer equipped with 1800 lines mm⁻¹, microscope objective of x100 and acquisition of 10s per 30 cycles.

The ⁵⁷Fe-Mössbauer spectra were obtained at room temperature in the standard transmission geometry in the constant acceleration mode using a ⁵⁷Co(Rh) radioactive source. The velocity scale was calibrated by the spectrum of alpha iron foil. The Mössbauer spectra were fitted by WinNormos software package (Brand 2008). The isomer shift values (δ) are given relative to α -Fe ($\delta = 0$).

The Cd^{2+} , Ni^{2+} , Cr(VI) and phosphate ions concentrations in the solutions after the adsorption and kinetic experiments were analyzed by a PinAAcle 900T Atomic Absorption Spectrometer. The mean value from three adsorption experiments was used for processing of experimental data.

Results and discussion

ATR-FTIR analysis

ATR-FTIR spectra of the unmodified and MG modified WL-based adsorbents are shown in Fig. 2. The bands characteristic for WL containing ceramics observed at 994 cm^{-1} , 1110 cm^{-1} originate from stretching bridging Si–O(Si) vibrations, while bands at 897 cm^{-1} , 874 cm^{-1} , and 846 cm^{-1} originates from stretching non-bridging Si–O vibrations (Obradović et al. 2017a). The low intensity band at 714 cm^{-1} originates from stretching vibration of Si–O(Si) bridging bond, which is characteristic for the presence of a 3-membered ring in WL ceramics. The intense band at 1410 cm^{-1} is assigned to the carbonate ion vibrational modes in bulk calcite. Broad band around $3300\text{--}3500\text{ cm}^{-1}$, observed in ATR-FTIR spectra of WL/DA, originates from hydroxyl group (OH) stretching vibration. The bands at 2930 cm^{-1} and 2870 cm^{-1} originate from symmetric and asymmetric stretching vibrations of methylene group. Moreover, the absorption peaks at 1680 cm^{-1} and 1580 cm^{-1} originates from amide I stretching vibrations, and N-H deformation vibrations coupled with $\nu(\text{C-N})$ vibrations (amide II), respectively.

The low intensity peak around 564 cm^{-1} observed in the ATR-FTIR spectrum of WL/MG and WL- γ -APS/MG originates from vibration of the $\text{Fe}^{2+}\text{--O}^{2-}$ functional group (Khalil 2015) overlapped with the peaks which originate from the C–C=O and C–N–C vibrations (DETAPA moiety in WL- γ -APS/MG sample). Raman spectroscopy and ^{57}Fe -Mössbauer analysis are more suitable techniques for quantification of the amount of MG doped on WL containing ceramics, as well as the determination of the phase and composition of the deposit.

Fig. 2.

Raman analysis

Raman spectra of the unmodified and modified (direct/via γ -APS/DA cross-linker) WL based adsorbents are shown in Fig.3. In the Raman spectrum of unmodified WL peaks that originate from both bare WL and β -larnite are noticed. The peak assignation is done according to the literature data and it is shown in Fig.3 (Swamy et al. 1997; Richet et al. 1998; Ricciardi et al. 2009; Sokol et al. 2015). The small intensity peak at 1083 cm^{-1} indicates that there are residual CaCO_3 in WL structure (White 2009; Ricciardi et al. 2009).

In the Raman spectra of both modified WL samples, *i.e.* WL/MG and WL- γ -APS/MG, two wide peaks of magnetite, followed by two low intensity peaks of maghemite, are observed (de Faria et al. 1997; Ovsyannikov et al. 2010; Li et al. 2012). Partial transformation of magnetite into maghemite is found to induced by laser excitation (de Faria et al. 1997). The WL peaks at $< 500\text{ cm}^{-1}$ can be assigned to the Ca–O stretching (the lowest frequencies in the region) and bending vibrations (higher frequencies in the region). On the other hand, Raman signals of WL observed between 500 and 600 cm^{-1} originate from the O–Si–O bending vibrations. Although the

band at 635 cm^{-1} can be attributed to the Si-O-Si bending vibration (Osticioli et al. 2009; Buzatu and Buzgar 2010; Ebbert et al. 2014), some authors point out that this peak originates from the Si-O_{br} stretching vibrations, where O_{br} presents bridging oxygen. The stretching Si-O_{br} vibrations induce also the occurrence of the peak between 650 and 750 cm^{-1} , while Raman peaks between 850 and 200 cm^{-1} can be assigned to the Si-O nonbridging stretching vibrations (Si-O_{nbr}).

Fig. 3.

XRD analysis

XRD patterns of sintered unmodified WL and modified WL samples, WL/MG and WL- γ -APS/MG, are presented in Fig.4. All obtained intensities are identified by JCPDS cards (042-0547 for wollastonite CaSiO_3 , and 077-0409 for larnite Ca_2SiO_4). A two-phase system is detected in unmodified WL samples: wollastonite and larnite (13.4 % CaSiO_3 and 86.6 % Ca_2SiO_4). Peaks for magnetite, marked by their indices [(111), (220), (311), (400), (422), (511), (440)] (Wang et al. 2009; Huang et al. 2017), are observed in XRD curves for both WL/MG and WL- γ -APS/MG samples. No additional peaks are observed.

Fig.4.

^{57}Fe -Mössbauer spectroscopy

The ^{57}Fe -Mössbauer spectra of modified WL samples, W- γ -APS/MG and W-MG, are presented in Fig.5. The samples were evaluated using WinNormos-DIST program. The two absorption lines (so called a doublet) were visible in the WL- γ -APS/MG spectrum. The spectrum was fitted with the distribution of the quadrupole splitting. The distribution was described using histogram distribution of 30 doublets of Lorentzian lines with the same FWHM (0.3 mms^{-1}) in steps of 0.1 mms^{-1} . The linear correlation between the quadrupole splitting and the isomer shift was applied. Isomer shifts for the quadrupole distribution covered range from ~ 0.33 to $\sim 0.34\text{ mms}^{-1}$. The quadrupole splitting distribution $P(\Delta)$ of the WL- γ -APS/MG sample is presented in Fig.6. In the WL/MG spectrum, besides the dominant central doublet, a broad six-lines absorption feature (so called a sextet) representing the magnetic contribution to the spectrum was also visible. The spectrum was fitted with one discrete doublet and one distribution of the hyperfine magnetic field (distribution of the magnetic splitting). The distribution of the magnetic splitting was described using a histogram distribution of 35 sextets of Lorentzian lines with the same FWHM (0.5 mms^{-1}) from 15 T in steps of 1 T. The linear correlation between the hyperfine magnetic field and the isomer shift was applied. Isomer shifts for the magnetic distribution covered the range from ~ 0.32 to $\sim 0.64\text{ mms}^{-1}$. The quadrupole shift was fixed to zero. The hyperfine magnetic field distribution $P(B_{\text{hf}})$ of the magnetic part of the WL/MG sample is presented in Fig. 7. In the same DIST program, one discrete doublet was combined with the magnetic distribution. The ^{57}Fe -Mössbauer parameters of the WL/MG and WL- γ -APS/MG samples are presented in Table 1. Under the assumption that f -factors of Fe atoms at various sites in the particular sample are identical, the area of the corresponding Mössbauer subspectrum was used to access the relative fractions of iron atoms at different sites.

Fig. 5.

Fig. 6.

Fig. 7.

The stoichiometric magnetite has an inverse spinel crystal structure. The tetrahedral sites (A-sites) are occupied by Fe^{3+} ions and the octahedral sites (B-sites) by the Fe^{3+} and Fe^{2+} ions. The site distribution in the MG structure is usually presented by the formula $(\text{Fe}^{3+})^A (\text{Fe}^{3+} \text{Fe}^{2+})^B \text{O}^{2-}_4$. At the temperatures above the Verwey transition temperature (~ 119 K), a rapid electron exchange exist between the Fe^{2+} and Fe^{3+} ions at the B-sites which leads to the effective $\text{Fe}^{2.5+}$ valence (Kündig and Steven Hargrove 1969, and references therein). Depending on the amount of the Fe^{2+} in the MG structure, the so called non-stoichiometric $\text{Fe}_{3-x}\text{O}_4$ or partially oxidized MG can have a range of oxidation states (Gorski and Scherer 2010; Kalska-Szostko et al. 2015). Vacancies are formed in the MG structure (presumably on the octahedral sites) to account for the charge balance. The structure of the completely oxidized MG ($x = 1/3$) is the crystal structure of the maghemite, $\gamma\text{-Fe}_2\text{O}_3$. At the room temperature (RT), only two magnetic sextets are observed in the Mössbauer spectrum of pure bulk MG (Kündig and Steven Hargrove 1969; da Costa 1995; Stevens et al. 2005; Dyar et al. 2006). The first sextet that belong to the A-site has the hyperfine magnetic field $B_{\text{hf}} \sim 49$ T and the isomer shift value characteristic for the Fe^{3+} ions $\delta \sim 0.27$ mms^{-1} . The second sextet comprises all the iron B-sites and, due to the electron hopping between iron B-sites, exhibit the hyperfine magnetic field $B_{\text{hf}} \sim 46$ T with lines broadened and shows an isomer shift of around $\delta \sim 0.67$ mms^{-1} - an averaged value of the isomer shift values for the Fe^{2+} and Fe^{3+} ions at B-sublattice. The ratio of the A to B sextets is 1:2. For the maghemite, the two sextets have very close values of the hyperfine magnetic fields, so only one sextet of $B_{\text{hf}} \sim 50$ T and isomer shift around $\delta \sim 0.32$ mms^{-1} is seen in the bulk maghemite Mössbauer spectrum at RT (Stevens et al. 2005; Dyar et al. 2006). For a partially oxidized MG or for the mixture of MG and maghemite, the relative intensities of the two sextets change, but the parameters remain essentially the same (Joos et al. 2016; Fock et al. 2017). The well-defined magnetic splitting for MG and maghemite is seen at RT only for particles with the grain size larger than 15 nm and can serve as a basis for their phase differentiation. For smaller particle grains, the magnetic splitting may collapse to a singlet or doublet due to the superparamagnetic relaxation or sextet may be severely broadened (Roggwiller and Kundig 1973; daCosta et al. 1998; Dézsi et al. 2008; Suzdalev et al. 2012; Carvalho et al. 2013; Kalska-Szostko et al. 2015; Joos et al. 2016; Oshtrakh et al. 2016). Also, in the RT-Mössbauer spectrum, superparamagnetic (SPM)-magnetite nanoparticles are hard to be distinguished from the other SPM-iron-oxide/iron-hydroxide nanoparticles (Joos et al. 2016).

Table 1. Room temperature ^{57}Fe -Mössbauer hyperfine parameters for the WL/MG and WL- γ -APS/MG samples

| Sample | Mössbauer subspectrum | A (%) | Γ (mms^{-1}) | $\delta / \langle \delta \rangle$ (mms^{-1}) | $\Delta / \langle \Delta(\sigma) \rangle$ (mms^{-1}) | $\langle B_{\text{hf}}(\sigma) \rangle$ (T) |
|----------------------|-----------------------|-------|--------------------------------|---|---|---|
| WL/MG | D | 59 | 0.572(8) | 0.344(3) | 0.827(5) | |
| | B-distrib. | 41 | 0.5 | 0.42(9) | 0 | 39.1(7.6) |
| WL- γ -APS/MG | Q-distrib. | 100 | 0.3 | 0.339(5) | 0.76(0.38) | |

A – relative area of the Mössbauer subspectrum; Γ - line width (FWHM); δ – isomer shift; Δ - the quadrupole splitting. In the case of the distribution of the quadrupole splitting: $\langle \delta \rangle$ – average isomer shift; $\langle \Delta(\sigma) \rangle$ - average quadrupole splitting and standard deviation of the distribution of the quadrupole splitting. In case of the distribution of the magnetic splitting: $\langle \delta \rangle$ – average isomer shift; $\langle B_{\text{hf}}(\sigma) \rangle$ – average hyperfine magnetic field and standard deviation of the distribution of magnetic splitting. The fitting errors are presented in the parenthesis.

The calcium-based silicates may be also represented by the various doublets in the Mössbauer spectra at RT (Dowty and Lindsley 1973; Stevens et al. 2005; Dyar et al. 2006). The doublets with the isomer shift values of around 1 mms⁻¹ or higher that may represent Fe²⁺ ions incorporated in the calcium-silicates or silicates (Dowty and Lindsley 1973; Murad and Wagner 1998; Stevens et al. 2005; Dyar et al. 2006) could not be fitted to the WL-γ-APS/MG spectrum. In the case of the WL/MG, the Fe²⁺ doublet originated from calcium-silicates and silicates would be covered by the broadened sextet. On the other hand, the presence of the Fe³⁺ ions in silicates in the two investigated samples could not be excluded, since their Mössbauer parameters are in most cases overlapping with the ones of the SPM-iron-oxide/hydroxide nanoparticles (Murad and Wagner 1998; Stevens et al. 2005; Dyar et al. 2006). Nevertheless, despite the difficulties stated above, the most probably scenario for the two samples is that the majority of Fe is incorporated in the iron-oxide nanophase. The calcium-silicate phases present in the samples should exhibit an Fe²⁺ ion - Mössbauer signature as mentioned above, which could not be detected in significant amount for both samples. For the WL-γ-APS/MG spectrum, the fit that may distinguish between different phases in the WL-γ-APS/MG sample, *i.e.* the fit with two or more doublets could not provide a unique set of Mössbauer parameters. Therefore, we decided to fit the spectrum with one quadrupole splitting distribution. The average value of the quadrupole splitting distribution was ~0.76 mms⁻¹. Under assumptions that the majority of iron is incorporated into the iron-oxide nanoparticles, for the WL-γ-APS/MG sample, the waste majority of the ultra-fine iron-oxide nanoparticles are in the superparamagnetic state. Similar reasons apply for the RT WL/MG - ⁵⁷Fe-Mössbauer spectrum. The dominant doublet could be fitted to the WL/MG spectrum satisfactory with only one doublet and therefore may also incorporate both, the SPM-iron-oxides/hydroxides and/or the silicate phases. The WL/MG - ⁵⁷Fe-Mössbauer spectrum differs from the WL-γ-APS/MG spectrum in the presence of the magnetic contribution visible as the broadened asymmetrical sextet. The fits of the magnetic part of the WL/MG spectrum with the two magnetic field distributions for A- and B-site in MG phase were not satisfactory. Also the fits with one discrete sextet for the A-site and one magnetic field distribution for the B-site also failed to describe the spectrum reasonably. The magnetic component correlated with the A-site in the MG with $B_{hf} \sim 49$ T was not present in the spectrum. Finally, the magnetic part was fitted with one hyperfine magnetic field distribution (Fig. 7). Several peaks are present in the magnetic distribution for the WL/MG sample. An attempt to fit the probability distribution $P(B_{hf})$ with five Gaussian was made (Fig. 7): the most prominent peak is located at ~ 44.9 T ($\delta \sim 0.36$ mms⁻¹), followed by smaller maxima at 40.7 T ($\delta \sim 0.40$ mms⁻¹), 35.8 T ($\delta \sim 0.45$ mms⁻¹), 28.5 T ($\delta \sim 0.51$ mms⁻¹) and 21.7 T ($\delta \sim 0.58$ mms⁻¹). The peaks parameters do not indicate clearly to the specific iron-oxide/iron-hydroxide phase. Besides the above mentioned reasons associated with the reducing of the particle size, there may be several other reasons for the lowering of the hyperfine magnetic field at various Fe sites in the iron-oxide nanoparticles and broadening of the spectrum lines: significant distribution in the particles size, poorly crystallized nanoparticles, inclusion of various impurities/phases into the grains, etc.

Scanning electron microscopy (SEM)

The SEM micrographs of the synthesized PMMA microspheres, used as a pore-forming agent, and calcined unmodified and modified WL powders are shown in Fig. 8. From Fig. 8a) it can be observed that the soap-free emulsion polymerization produce PMMA microspheres with high uniform dimensions (~700-800 nm). During the calcination of the WL powder, PMMA

microspheres are subjected to degradation and evaporation which undergoes swelling and cause forming of non-uniform porous structure (Fig. 8b)). Inside WL structures, noticed pores are connected, as presented in Fig. 8b). Submicro-size PMMA particles, approximately 0.1-1.50 microns (Sreekanth Chakradhar et al. 2006; Obradović et al. 2017a), caused micro-porosity in obtained material. A comparative morphology study of direct and indirect MG modified WL shows that smaller MG agglomerates (Fig. 8d)) were precipitated using MG spheres attaching method *via* γ -APS/DA cross-linker. Clearly visible MG agglomerates with higher dimensions were obtained using the polyol-medium solvothermal method (Fig. 8c)).

These results were confirmed by EDS mapping and EDS image. The obtained results are shown in Fig.9 and Table S1. The EDS image proves the presence of the starting elements O, Si, Ca and Fe (Fig. 9 a) and b)). Moreover, the elemental mapping (O and Fe elements) shows clearly that direct attaching of MG spheres on WL led to the precipitation of MG agglomerates of higher dimensions, while attaching of MG spheres *via* γ -APS/DA cross-linker led to a more uniform precipitation of MG particles of smaller dimensions. This can be attributed to numerous nucleation/crystallization centers (carboxylic groups/carboxylate anions) suitable for iron complexation in the initial stage, while in the course of adsorbent synthesis MG precipitation take place by MG crystal growth producing a large number of more uniformly distributed smaller particle size on WL/DA surface (Fig.1). Numerous crystallization centers affect the MG loading. Hence, as shown in the results of the EDS analysis (Table S1), a higher loading of MG was bounded by precipitation *via* γ -APS/DA cross-linker (11.36%), while only 4.37% were bounded by direct MG precipitation. These results were corroborated by acidic dissolution in nitric acid and determination of iron content (10.66% for WL/ γ -APS/DA and 4.76% for WL/MG).

Fig. 8.

Fig.9.

Determination of the point of zero charge (pH_{PZC}) of wollastonite-based adsorbent and effect of pH on adsorption efficiency

The pH influences the state of equilibrium of ionic species and protonation/deprotonation of sorbent functional groups. The pH of the point of zero charge, pH_{PZC} for the magnetite modified WL based adsorbents was measured by the pH drift method. In aqueous systems, the surface of iron oxides is covered with FeOH groups that can be protonated or deprotonated and generate surface charge FeOH_2^+ or FeO^- at pH values below or above the point of zero charge for magnetite (pH_{PZC}), respectively (Rajput et al. 2016). Electrostatic forces between metal ion species and surface charges are responsible for adsorption (Ahmed et al. 2013; Rajput et al. 2016). The point of zero charge for magnetite is the pH value at which the surface concentrations of FeOH^{2+} and FeO^- groups are equal. The measured pH_{PZC} of unmodified WL was 2.7, while pH_{PZC} of both MG modified WL based adsorbents was ~ 7.0 . In the next step, the removal degree of Ni^{2+} and Cd^{2+} *versus* the initial pH (pH_i) was studied, and the obtained results are presented in Fig.S1. At low pH (lower than pH_{PZC} of MG modified WL), sorbent surface is covered mostly with FeOH^{2+} and positively charged surface functionalities. Therefore, the positively charged metal ions, Ni^{2+} and Cd^{2+} , showed low adsorption efficiency due to both the repulsive forces and the adsorption of H_3O^+ which hinders/competitively occupy adsorptive sites (Ahmed et al. 2013).

It can be noticed from Fig.S1 that, with an increase in pH from 3 to 9, the Cd^{2+} and Ni^{2+} percentage uptake increased too. In the pH range between 7 and 9 the maximum of Ni^{2+} and Cd^{2+} percentages uptake was observed (72 % and 97 % Cd^{2+} uptake on WL/MG and WL- γ -APS/MG, receptively, and 84 % and 85 % Ni^{2+} uptake on WL/MG and WL- γ -APS/MG, receptively). Subsequently gradual decrease of Cd^{2+} and Ni^{2+} uptake on was WL/MG and WL- γ -APS/MG observed at $\text{pH} > 8$. The variation in the effectiveness of metal removal at different pH values could be explained by metal speciation as shown in Fig. S2. From the speciation diagram of Cd^{2+} and Ni^{2+} ion (Fig.S2), obtained by using MINTEQ. 3.0 software (Gustafsson 2011), high removal efficiencies would be expected in the pH region 7-8 for both Cd^{2+} and Ni^{2+} , while adsorption capabilities at $\text{pH} > 8$ could originate from additional contribution of the precipitation of insoluble metal hydroxides (Drah et al. 2017). Thus adsorption curves for studied cations represent only adsorption with excluded precipitation at $\text{pH} > 8$. According to this, at $\text{pH} < 8$, it was certain that removals of Cd^{2+} and Ni^{2+} were not affected by hydroxide/salt precipitation, and obtained results were considered without any misleading conclusions (Drah et al. 2017). In this sense, the selection of pH 7.5 for Cd^{2+} and Ni^{2+} removal and pH 6.5 for both Cr(VI), considering equilibrium of $\text{HCrO}_4^-/\text{CrO}_4^{2-}$ ions, and phosphate, equilibrium of $\text{H}_2\text{PO}_4^-/\text{HPO}_4^{2-}$ ions, was an adequate choice to achieve high adsorption capacities.

Adsorption/desorption study of Cd^{2+} , Ni^{2+} , $\text{HCrO}_4^-/\text{CrO}_4^{2-}$ and $\text{H}_2\text{PO}_4^-/\text{HPO}_4^{2-}$ on WL/MG and WL- γ -APS/MG adsorbents

According to the previous adsorptions studies, it was confirmed that heavy metals undergo complexation and hydrolysis during adsorption (Kumari et al. 2015). Surface complexation of heavy metals occurs *via* exchange of metal ions M^{m+} with H^+ ions at the surface hydroxyl groups $-\text{M}'\text{OH}$. $\text{M}(\text{OH})_n^{(m-n)+}$ ions, that occurs during the hydrolysis, can electrostatically interact with the iron-oxide (MG) surfaces forming a specific type of adsorbed ion/surface interaction (Petrova et al. 2011). It was found that metals hydrolysis causes weakening of the interaction between the metal ion and water in hydration shell that facilitates the approach of the metal ions to the surface (Petrova et al. 2011).

However, analysis/description of adsorption mechanism of oxyanions is complex/extensive task and needs more reliable results, and most of them are based on spectroscopic evidence (Kumari et al. 2015). Multiple adsorption mechanisms occur during the phosphate ions up-taking. The cationic species ($\text{M}(\text{OH})_n^{(m-n)+}$) takes part in uptaking of phosphate ions via electrostatic interaction (Rout et al. 2015, 2016). However, it is proved that complexation of oxyanions on MG surface was achieved by formation of monodentate and bidentate complexes through covalent bonding between the surface oxide's oxygen and the adsorbing metal ion (Kumari et al. 2015). Three main forms of phosphate complexes on iron oxide surface were defined: protonated $((\text{FeO})_2(\text{OH})\text{PO})$, nonprotonated bridging bidentate $((\text{FeO})_2\text{PO}_2)$ and a nonprotonated monodentate $((\text{FeO})\text{PO}_3)$ (Tejedor-Tejedor and Anderson 1990). In a similar manner due to similar chemistry chromate, schematic illustration of formation of monodentate and bidentate complexes between MG modified WL and $\text{HCrO}_4^-/\text{CrO}_4^{2-}$ ions is presented on Fig. S3.

The state of interaction/bonding at solutes/sorbent surface can be described by fitting experimental data with various adsorption isotherms (Markovski et al. 2014b). Analysis of adsorption data was performed by using various isotherm models, and statistical criteria used to evaluate the quality of model fitting of adsorption data. The Langmuir isotherm model is given

by Eq. (2), while thermodynamic parameters for studied ions were first estimated using the Gibbs free energy equation and the linearized van't Hoff Equation (*i.e.*, the van't Hoff plot) as follows (Liu et al. 2015):

$$q_e = (Kq_{\max}C_e)/(1 + KC_e) \quad (2)$$

$$\Delta G^o = -RT \ln K_L \quad (3)$$

$$\ln K_L = -\frac{\Delta H^o}{RT} + \frac{\Delta S^o}{R} \quad (4)$$

where: C_e is the equilibrium concentration of ion at equilibrium (mol l^{-1}), q_e is the amount of ions adsorbed per weight unit of solid at equilibrium (mol g^{-1}), K and K_L are Langmuir constants related to sorption affinity in l mg^{-1} and l mol^{-1} , respectively, and q_{\max} is maximum sorption capacity (mol g^{-1}), ΔG^o (kJ mol^{-1}) is the change of free energy, ΔH^o (kJ mol^{-1}) is the change of enthalpy, ΔS^o (kJ mol^{-1}) is the change of entropy, T (K) is the absolute temperature and R is the ideal gas constant ($0.008314 \text{ kJ mol}^{-1} \text{ K}^{-1}$). The values of non-linear Langmuir adsorption isotherm and thermodynamic parameters at 298, 308 and 318 K for Cd^{2+} , Ni^{2+} , $\text{HCrO}_4^-/\text{CrO}_4^{2-}$ and $\text{H}_2\text{PO}_4^-/\text{HPO}_4^{2-}$ ions adsorption, using WL/MG and WL- γ -APS/MG adsorbents, are presented in Tables 2 and 3, and Fig. S4. Linear Langmuir adsorption isotherms, as well as values of the q_e , K and K_L are presented in Fig. S5, and Tables S2 and S3.

According to the Langmuir isotherm, mechanism of Cd^{2+} , Ni^{2+} , $\text{HCrO}_4^-/\text{CrO}_4^{2-}$ and phosphate ions adsorption onto WL/MG and WL- γ -APS/MG sorbents can be described by monolayer adsorption with equal energy and enthalpy for all adsorption sites. Langmuir isotherm assumed that the energy of adsorption is generally considerably larger than for the second and higher layers, and therefore multilayer formation is less possible (Rouquerol et al. 1999).

The results presented in Table 2 show high predicted adsorption capacity for both WL/MG and WL- γ -APS/MG adsorbents, and increase of adsorption capacity with the temperature increase. Moreover, adsorption results significantly support better adsorption performances of WL- γ -APS/MG (26.7 – 33.0 % higher q_e) due to developed surface formed by size- and distribution controllable deposition of MG on WL/DA.

The higher values of the Langmuir constant, that reflect the sorption affinity, were obtained for adsorption of all ions on WL- γ -APS/MG adsorbents at all temperatures. Higher temperature dependence was obtained for $\text{H}_2\text{PO}_4^-/\text{HPO}_4^{2-}$ and $\text{HCrO}_4^-/\text{CrO}_4^{2-}$ oxyanions, which means higher probability of surface complexation at higher temperature. Comparing obtained values of the Langmuir constant it can be concluded that WL/MG and WL- γ -APS/MG adsorbents have higher sorption affinity for Ni^{2+} and Cd^{2+} as a results of their bonding mechanism. It can be explained by complex formation of monodentate mononuclear and bidentate binuclear complexes of $\text{HCrO}_4^-/\text{CrO}_4^{2-}$ and $\text{H}_2\text{PO}_4^-/\text{HPO}_4^{2-}$ ions with MG surface hydroxylic groups, while Ni^{2+} and Cd^{2+} ions easily create electrostatic interactions with MG centers. Moreover, the complexation of all investigated pollutant is easier with developed surface of W- γ -APS/MG adsorbent.

Table 2. Non-linear Langmuir isotherm parameters for Cd^{2+} , Ni^{2+} , $\text{H}_2\text{PO}_4^-/\text{HPO}_4^{2-}$ and $\text{HCrO}_4^-/\text{CrO}_4^{2-}$ ions obtained at 298, 308 and 318 K using WL/MG and WL- γ -APS/MG adsorbents

| | Cd^{2+} | | | | Ni^{2+} | | |
|--------------------------------------|------------------|---------------------------------|-------------------------------|-------|---------------------------------|-------------------------------|-------|
| | $T(\text{K})$ | q_e (mg g^{-1}) | K (l mg^{-1}) | R^2 | q_e (mg g^{-1}) | K (l mg^{-1}) | R^2 |
| WL/MG | 298 | 50.543 | 24.313 | 0.960 | 47.889 | 23.330 | 0.936 |
| | 308 | 53.429 | 22.389 | 0.922 | 50.216 | 22.856 | 0.909 |
| | 318 | 55.450 | 25.867 | 0.969 | 52.019 | 26.911 | 0.969 |
| WL-γ-APS/MG | 298 | 69.289 | 19.096 | 0.876 | 61.412 | 24.638 | 0.989 |
| | 308 | 69.724 | 44.152 | 0.986 | 63.076 | 28.920 | 0.979 |
| | 318 | 73.126 | 61.886 | 0.986 | 66.144 | 37.083 | 0.988 |

| | $\text{H}_2\text{PO}_4^-/\text{HPO}_4^{2-}$ | | | | $\text{HCrO}_4^-/\text{CrO}_4^{2-}$ | | |
|--------------------------------------|---|---------------------------------|-------------------------------|-------|-------------------------------------|-------------------------------|-------|
| | T (K) | q_e (mg g^{-1}) | K (l mg^{-1}) | R^2 | q_e (mg g^{-1}) | K (l mg^{-1}) | R^2 |
| WL/MG | 298 | 44.529 | 17.021 | 0.943 | 42.824 | 14.940 | 0.844 |
| | 308 | 46.262 | 19.060 | 0.947 | 44.447 | 13.262 | 0.808 |
| | 318 | 48.132 | 19.637 | 0.962 | 47.382 | 14.477 | 0.829 |
| WL-γ-APS/MG | 298 | 60.019 | 35.202 | 0.957 | 62.133 | 12.071 | 0.903 |
| | 308 | 62.702 | 35.921 | 0.981 | 63.632 | 19.354 | 0.917 |
| | 318 | 64.168 | 38.153 | 0.965 | 63.456 | 37.923 | 0.973 |

Table 3. Thermodynamic parameters Cd^{2+} , Ni^{2+} , $\text{H}_2\text{PO}_4^-/\text{HPO}_4^{2-}$ and $\text{HCrO}_4^-/\text{CrO}_4^{2-}$ ions obtained at 298, 308 and 318 K using WL/MG and WL- γ -APS/MG adsorbents

| | Cd^{2+} | | | | Ni^{2+} | | |
|--------------------------------------|------------------|--|--|---|--|--|---|
| | T (K) | ΔG° (kJ mol^{-1}) | ΔH° (kJ mol^{-1}) | ΔS° ($\text{J mol}^{-1} \text{K}^{-1}$) | ΔG° (kJ mol^{-1}) | ΔH° (kJ mol^{-1}) | ΔS° ($\text{J mol}^{-1} \text{K}^{-1}$) |
| WL/MG | 298 | -45.23 | 2.15 | 159.10 | -45.20 | 2.01 | 158.75 |
| | 308 | -47.01 | | | -47.01 | | |
| | 318 | -48.40 | | | -48.36 | | |
| WL-γ-APS/MG | 298 | -46.21 | 12.64 | 198.04 | -45.19 | 9.32 | 183.33 |
| | 308 | -48.80 | | | -47.48 | | |
| | 318 | -50.14 | | | -48.83 | | |

| | $\text{H}_2\text{PO}_4^-/\text{HPO}_4^{2-}$ | | | | $\text{HCrO}_4^-/\text{CrO}_4^{2-}$ | | |
|--------------------------------------|---|--|--|---|--|--|---|
| | T (K) | ΔG° (kJ mol^{-1}) | ΔH° (kJ mol^{-1}) | ΔS° ($\text{J mol}^{-1} \text{K}^{-1}$) | ΔG° (kJ mol^{-1}) | ΔH° (kJ mol^{-1}) | ΔS° ($\text{J mol}^{-1} \text{K}^{-1}$) |
| WL/MG | 298 | -39.61 | 8.69 | 161.88 | -41.34 | 5.36 | 156.65 |
| | 308 | -41.11 | | | -42.92 | | |
| | 318 | -42.86 | | | -44.48 | | |
| WL-γ-APS/MG | 298 | -40.09 | 29.10 | 231.46 | -40.69 | 21.50 | 208.95 |
| | 308 | -41.89 | | | -43.13 | | |
| | 318 | -44.79 | | | -44.85 | | |

The negative ΔG° values indicate that adsorption occurs via spontaneous reactions (Veličković et al. 2012). Structure and stability of multilayered hydrated ions, charged or neutral, depend on pH and temperature. Changes in pH value dictate presence of ionic species which in turn affect structure/extent of interaction in hydration shell. Desolvation and diffusion at higher

temperatures are more feasible processes, which are noticed as slight ΔG° increase with temperature increase. According to general rules, the change of ΔG° for physisorption lies between -20 and 0 kJ mol⁻¹, both physisorption and chemisorption in the range from -20 to -80 kJ mol⁻¹, while the chemisorption between -80 and -200 kJ mol⁻¹. Obtained results indicate contribution of both physisorption and chemisorption (Vuković et al. 2010, 2011; Budimirović et al. 2017).

The positive ΔH° also indicates the endothermic nature of adsorption for all studied ions (Liu et al. 2015) (Table 3). The ΔH° does not significantly vary between cations adsorption on WL/MG, while slightly increases for Cd²⁺ adsorption on WL- γ -APS/MG. The highest ΔH° values are obtained for WL- γ -APS/MG for oxyanions. Low endothermic nature reflect low energy released/consumed by desolvation of cation and formation of an M²⁺/surface interactions, which could at appropriate balance. Higher ΔH° for oxyanions adsorption indicates higher energetic contribution of surface reaction, and diffusional processes at lower extent. All of these contributing elementary processes are individually low to significant, and could be either exothermic or endothermic, and their summary effect was found to be low endothermic.

The positive ΔS° relates to desolvation of structurally ordered hydronium ion and subsequent increase in randomness with increased concentration of adsorbed ions on the solid surface (Liu et al. 2015). Water molecules in surrounding solvation shell of metal ion form ordered structure, which after disruption of hydrogen-bonding increase system disorder. Positive values of entropy change (ΔS°) indicate the increase in disorder (randomness) on boundary solid-liquid surface. The M²⁺/surface interactions and oxyanions complexes formation means decrease in translational, rotational and vibrational motion which contributes to entropy decrease. Simultaneously, ΔS° increases due to both liberation of water due to adsorption and from cation hydration shell.

Except for this, results of reusability study showed low decrease of adsorption efficiency after three adsorptions/desorption cycles. An adsorption efficiency decrease of 22 %, 20 %, 25 % and 18 % for Cd²⁺, Ni²⁺, HCrO₄⁻/CrO₄²⁻ and H₂PO₄⁻/HPO₄²⁻ ions, respectively, was obtained after the third adsorption/desorption cycle using WL/MG adsorbent. Hence, lower decrease of adsorption efficiency of 18 %, 17 %, 19 % and 13 % for Cd²⁺, Ni²⁺, HCrO₄⁻/CrO₄²⁻ and H₂PO₄⁻/HPO₄²⁻ ions, respectively, was obtained after the third adsorption/desorption cycle using WL- γ -APS/MG adsorbent. According to this, it can be concluded that modification of WL based ceramic (support) with magnetic iron-oxide form (magnetite) *via* γ -APS/DA cross-linker gave adsorbent with higher stability of MG deposit. Moreover, with proper selection of technology for treatment of spent waste alkali concentrated Cd²⁺, Ni²⁺, HCrO₄⁻/CrO₄²⁻ and H₂PO₄⁻/HPO₄²⁻ ions provide safe technology for their removal.

Competitive adsorption study of Cd²⁺, Ni²⁺, HCrO₄⁻/CrO₄²⁻ and H₂PO₄⁻/HPO₄²⁻ ions removal from real water sample

Evaluation of WL/MG and WL- γ -APS/MG adsorbents potential use for Cd²⁺, Ni²⁺, HCrO₄⁻/CrO₄²⁻ and H₂PO₄⁻/HPO₄²⁻ ions removal from real water samples, contaminated natural water from the area of the city of Zrenjanin (located in Vojvodina, Serbia), was used for sorption experiment before any purification treatment. Other anions of interest presents in water sample are SO₄²⁻ (42.5ppm) and Cl⁻ (1.2 ppm) (Taleb et al. 2016b). Kinetic experiments performed with

100 ppm of WL/MG and WL- γ -APS/MG adsorbents were carried out to find out the level of the efficiency of total Cd^{2+} , Ni^{2+} , $\text{HCrO}_4^-/\text{CrO}_4^{2-}$ and $\text{H}_2\text{PO}_4^-/\text{HPO}_4^{2-}$ ions removal in natural water sample. It was found that competition of SO_4^{2-} and Cl^- ions was negligible (Petrova et al. 2011).

Adsorption kinetic study

Effect of time on pollutant adsorption was studied in a batch system containing m/V 125 mg l^{-1} of adsorbent at pH of 6.5 ± 0.10 for Cd^{2+} and Ni^{2+} and of 7.5 ± 0.10 for $\text{HCrO}_4^-/\text{CrO}_4^{2-}$ and $\text{H}_2\text{PO}_4^-/\text{HPO}_4^{2-}$ ions. The ions concentration was determined after 5, 10, 15, 30, 60, and 90 min. In order to properly describe adsorption kinetic, the obtained experimental data was fitted using different kinetic rate equations (Bizerea Spiridon and Pitulice 2014). According to the highest values of correlation coefficient, R^2 , which is a measure of conformity between experimental data and calculated ones, it was proved that pseudo-second-order (PSO), *i.e.* Eq. (5), was the most appropriate model for description of kinetic processes for both WL/MG and WL- γ -APS/MG adsorbents (Tables 4 and S4, Fig. S6 (linear) and S7 (non-linear fit)):

$$\frac{dq_t}{dt} = k_2(q_e - q_t)^2 \quad (5)$$

The adsorption capacities at equilibrium and at time t (min) are defined by q_e and q_t (mg g^{-1}) respectively, k_2 is the PSO rate constant ($\text{g mg}^{-1} \text{min}^{-1}$). The kinetic parameters, presented in Table 4, showed that both sorbents, and preferentially WL- γ -APS/MG, possess high affinity with respect to studied ions, and satisfactory rate at which system attain its equilibrium. According to pseudo second-order kinetic law, the rate limiting step may be chemical adsorption involving valent forces through sharing or the exchange of electrons between the sorbents and divalent metal ions (Qiu et al. 2009). The analysis of kinetic data, using PSO kinetic method, resulted in significantly higher rate constant (1.17 to 13.4 times higher) and relatively balanced values of adsorption capacity of studied ions using WL- γ -APS/MG adsorbent at all temperatures. The k_2 values increase with the increasing the temperature and the highest values are obtained at 318 K. These results indicate more efficient diffusional transport/adsorbate complexation at adsorbent surface *versus* temperature increase. Determination of activation parameters could give information on both energetic requirements to overcome slowest adsorption step and adsorption mechanism. The energy of activation (E_a) was calculated from the linear plot of the values of logarithms of rate constants (k_2) *versus* $1/T$ obtained by linearization of Arrhenius equation (Eq. 6) (results obtained in kinetic study at 298 K using the Eq. (5) (March 1985):

$$k_2 = Ae^{-(E_a/RT)} \quad (6)$$

Adsorption kinetics is generally controlled by diffusive mass transfer, thus rates of approaching to equilibrium usually increase with increasing of temperature. For the cations adsorption on both adsorbents, the results show that the intra-particle diffusion is a rate-controlling step since the activation energy is low and within the range of 6–17.5 kJ mol^{-1} characteristic for diffusion-controlled processes (Haring 1942). The higher activation energies for the adsorption of oxyanions reflect significance of morphological/porosity factor to improved adsorption kinetic.

Table 4. Kinetic and activation parameters obtained by the use of non-linear PSO kinetic model for the Cd^{2+} , Ni^{2+} , $\text{HCrO}_4^-/\text{CrO}_4^{2-}$ and $\text{H}_2\text{PO}_4^-/\text{HPO}_4^{2-}$ removal using WL/MG and WL- γ -APS/MG adsorbents

| 298 K | | | |
|----------------------|---|---|-------------------------------------|
| | Pseudo-second order | Cd^{2+} | Ni^{2+} |
| WL/MG | $k_2 \times 10^2$ (g mg ⁻¹ min ⁻¹) | 0.193±0.029 | 0.208±0.009 |
| | q_e (mg g ⁻¹) | 55.878±1.003 | 54.618±1.125 |
| | R^2 | 0.960 | 0.973 |
| | E_a (kJ mol ⁻¹) | 11.43 | 17.38 |
| WL- γ -APS/MG | $k_2 \times 10^2$ (g mg ⁻¹ min ⁻¹) | 1.222±0.021 | 1.187±0.005 |
| | q_e (mg g ⁻¹) | 70.027±1.112 | 62.563±1.082 |
| | R^2 | 0.992 | 0.991 |
| | E_a (kJ mol ⁻¹) | 20.78 | 24.20 |
| | Pseudo-second order | $\text{H}_2\text{PO}_4^-/\text{HPO}_4^{2-}$ | $\text{HCrO}_4^-/\text{CrO}_4^{2-}$ |
| WL/MG | $k_2 \times 10^2$ (g mg ⁻¹ min ⁻¹) | 0.594±0.012 | 0.248±0.017 |
| | q_e (mg g ⁻¹) | 42.819±1.124 | 46.982±1.115 |
| | R^2 | 0.927 | 0.972 |
| | E_a (kJ mol ⁻¹) | 13.91 | 27.12 |
| WL- γ -APS/MG | $k_2 \times 10^2$ (g mg ⁻¹ min ⁻¹) | 1.018±0.010 | 1.215±0.020 |
| | q_e (mg g ⁻¹) | 60.638±0.719 | 59.574±1.108 |
| | R^2 | 0.947 | 0.952 |
| | E_a (kJ mol ⁻¹) | 28.92 | 25.02 |
| 308 K | | | |
| | Pseudo-second order | Cd^{2+} | Ni^{2+} |
| WL/MG | $k_2 \times 10^2$ (g mg ⁻¹ min ⁻¹) | 0.223±0.012 | 0.238±0.001 |
| | q_e (mg g ⁻¹) | 59.445±0.748 | 58.931±1.197 |
| | R^2 | 0.988 | 0.975 |
| WL- γ -APS/MG | $k_2 \times 10^2$ (g mg ⁻¹ min ⁻¹) | 2.075±0.007 | 2.030±0.007 |
| | q_e (mg g ⁻¹) | 69.883±1.221 | 62.411±1.223 |
| | R^2 | 0.999 | 0.998 |
| | Pseudo-second order | $\text{H}_2\text{PO}_4^-/\text{HPO}_4^{2-}$ | $\text{HCrO}_4^-/\text{CrO}_4^{2-}$ |
| WL/MG | $k_2 \times 10^2$ (g mg ⁻¹ min ⁻¹) | 0.785±0.003 | 0.282±0.001 |
| | q_e (mg g ⁻¹) | 45.300±1.022 | 47.734±1.690 |
| | R^2 | 0.994 | 0.995 |
| WL- γ -APS/MG | $k_2 \times 10^2$ (g mg ⁻¹ min ⁻¹) | 2.452±0.008 | 2.402±0.003 |
| | q_e (mg g ⁻¹) | 61.336±1.103 | 62.494±0.426 |
| | R^2 | 0.973 | 0.947 |
| 318 K | | | |
| | Pseudo-second order | Cd^{2+} | Ni^{2+} |
| WL/MG | $k_2 \times 10^2$ (g mg ⁻¹ min ⁻¹) | 0.258±0.007 | 0.324±0.001 |
| | q_e (mg g ⁻¹) | 54.621±2.686 | 55.410±1.303 |
| | R^2 | 0.997 | 0.986 |
| WL- γ -APS/MG | $k_2 \times 10^2$ (g mg ⁻¹ min ⁻¹) | 2.068±0.002 | 2.183±0.008 |
| | q_e (mg g ⁻¹) | 73.092±0.299 | 65.730±0.987 |
| | R^2 | 0.992 | 0.979 |
| | Pseudo-second order | $\text{H}_2\text{PO}_4^-/\text{HPO}_4^{2-}$ | $\text{HCrO}_4^-/\text{CrO}_4^{2-}$ |
| WL/MG | $k_2 \times 10^2$ (g mg ⁻¹ min ⁻¹) | 0.851±0.004 | 0.496±0.001 |
| | q_e (mg g ⁻¹) | 46.939±1.001 | 47.402±1.112 |
| | R^2 | 0.966 | 0.939 |
| WL- γ -APS/MG | $k_2 \times 10^2$ (g mg ⁻¹ min ⁻¹) | 2.097±0.004 | 2.332±0.004 |
| | q_e (mg g ⁻¹) | 63.999±0.682 | 63.184±0.636 |
| | R^2 | 0.899 | 0.993 |

The kinetic data results (Table S5) obtained by applying Weber–Morris (W-M) kinetic model were useful in evaluation of rate limiting step of overall process (Vuković et al. 2011). High values of W-M constant C_1 for both cations and oxyanions (Table S5) indicate that intra-particle diffusion is not the only rate-limiting step; complex influence of the other factors determine effectiveness of overall pollutant transport. At the initial stage of the process, the diffusion from bulk phase to the exterior surface takes place at high rate, while second linear part, which depends on material porosity, relate to the diffusion inside mesopores/micropores.

Various adsorbents for Cd^{2+} , Ni^{2+} , $\text{HCrO}_4^-/\text{CrO}_4^{2-}$ and $\text{H}_2\text{PO}_4^-/\text{HPO}_4^{2-}$ ions removal, including unmodified and iron-oxide modified materials such as activated carbon, clays, cellulose based materials and WL based sorbents were reported in literature (Vuković et al. 2010; Karnib et al. 2014; Taleb et al. 2016b). Cd^{2+} , Ni^{2+} , $\text{HCrO}_4^-/\text{CrO}_4^{2-}$ and $\text{H}_2\text{PO}_4^-/\text{HPO}_4^{2-}$ ions adsorption capacities (value of q_e derived from Langmuir equation) of various WL and magnetite based adsorbents are summarized in Table S6. According to the presented Cd^{2+} , Ni^{2+} , $\text{HCrO}_4^-/\text{CrO}_4^{2-}$ and $\text{H}_2\text{PO}_4^-/\text{HPO}_4^{2-}$ ions adsorption capacities on WL and MG based adsorbents, with regard to other equilibrium contact times, the applied adsorbent in the present study could potentially be used as efficient adsorbent to remove Cd^{2+} , Ni^{2+} , $\text{HCrO}_4^-/\text{CrO}_4^{2-}$ and $\text{H}_2\text{PO}_4^-/\text{HPO}_4^{2-}$ ions from aqueous solutions in a short time period. Both, bare WL and MG nanoparticles showed moderate adsorption capacities ($6.5 - 13.5 \text{ mg g}^{-1}$) for Cd^{2+} , Ni^{2+} , $\text{HCrO}_4^-/\text{CrO}_4^{2-}$ and $\text{H}_2\text{PO}_4^-/\text{HPO}_4^{2-}$ ions removal. Moreover, hybrid adsorbents obtained by MG precipitation on porous WL support showed higher adsorption capacities ($52.41 - 73.15 \text{ mg g}^{-1}$) due to availability of more active sites for heavy metals removal and oxyions complexation.

Monolayer model for single-compound adsorption

For the monolayer model for single-compound adsorption it is assumed that heavy metal ions/oxyanions are adsorbed with one energy ($-\varepsilon$) (Sellaoui et al. 2017a). The $-\varepsilon$ describes the interaction of ions with the surface of the MG-modified WL-based sorbents. **Adsorption energy is calculated according to the following equation (Sellaoui et al. 2017b):**

$$\varepsilon = k_B T \ln \left(\frac{c_s}{c_{1/2}} \right) \quad (7)$$

where k_B Boltzmann constant, c_s is the solubility of the heavy metal and $c_{1/2}$ is the concentration at half saturation (Sellaoui et al. 2016b, a). According to the general Langmuir model interpretation, each adsorption site accommodates one ion, as following chemical pseudo-reactions **describe** (Sellaoui et al. 2017b, a):



where A^{2+} represents the adsorbed Cd^{2+} or Ni^{2+} ions, S is the adsorbent receptor site, $\text{A}^{2+}n\text{S}$ represents formed complex of cations with MG-modified WL-based sorbents, n represents number of the bonded ions per one receptor site, B^- and B^{2-} **represent** the mono- and divalent chromate or phosphate oxyanions, and B^-nS and $\text{B}^{2-}n\text{S}$ represent formed complexes of oxyanions

with MG-modified WL-based sorbents. The partition function of one identical site and the monolayer model for single-compound adsorption are described by following equations:

$$Z_{gc} = 1 + e^{\beta(\varepsilon+\mu)} \quad (11)$$

$$Z_{gc} = e^{\beta(\varepsilon+\mu)N_M} \quad (12)$$

$$Q = \frac{nN_M}{1+\left(\frac{c_{1/2}}{c}\right)^n} \quad (13)$$

In these expressions, ε represents the adsorption energy of the receptor site, μ is the chemical potential of the adsorbed state determined from the Gibbs free energy, β is the Boltzmann factor, defined as $1/(k_B T)$, Q is the adsorption capacity, n is the number of ions per site, N_M is the density of receptor site, and c is the heavy metal ion/oxyanion equilibrium concentration (Sellaoui et al. 2016b, a). Different values for the parameters for single-compound adsorption of heavy metal ions/oxyanions on MG-modified WL-based sorbents are presented in Table 5.

Table 5. Values of adjustable parameters in single-compound system for adsorption of Cd^{2+} , Ni^{2+} , $\text{HCrO}_4^-/\text{CrO}_4^{2-}$ and $\text{H}_2\text{PO}_4^-/\text{HPO}_4^{2-}$ ions

| | Cd^{2+} | | | | | Ni^{2+} | | | |
|----------------------|-------------------------------------|--------------------------------------|-------------------------------------|--------------------------|------|---|-------------------------------------|--------------------------|------|
| | T (K) | ε , (KJ mol $^{-1}$) | Q_{sat} (mg g $^{-1}$) | N_M (mg g $^{-1}$) | n | ε , (KJ mol $^{-1}$) | Q_{sat} (mg g $^{-1}$) | N_M (mg g $^{-1}$) | n |
| WL/MG | 298 | 7.624 | 55.878 | 45 | 0.66 | 6.781 | 54.618 | 44 | 1.21 |
| | 308 | 7.967 | 59.445 | 45 | 0.85 | 7.108 | 58.931 | 44 | 0.91 |
| | 318 | 7.388 | 54.621 | 45 | 1.11 | 7.411 | 55.410 | 44 | 0.88 |
| WL- γ -APS/MG | 298 | 7.698 | 70.027 | 45 | 0.82 | 6.822 | 62.563 | 44 | 0.70 |
| | 308 | 8.024 | 69.883 | 43 | 0.96 | 7.126 | 62.411 | 43 | 0.99 |
| | 318 | 8.491 | 73.092 | 43 | 1.21 | 8.388 | 65.730 | 44 | 1.25 |
| | $\text{HCrO}_4^-/\text{CrO}_4^{2-}$ | | | | | $\text{H}_2\text{PO}_4^-/\text{HPO}_4^{2-}$ | | | |
| | T (K) | ε , (KJ mol $^{-1}$) | Q_{sat} (mg g $^{-1}$) | N_M (mg g $^{-1}$) | n | ε , (KJ mol $^{-1}$) | Q_{sat} (mg g $^{-1}$) | N_M (mg g $^{-1}$) | n |
| WL/MG | 298 | 6.310 | 46.982 | 49 | 0.65 | 6.059 | 42.819 | 53 | 0.58 |
| | 308 | 6.715 | 47.734 | 49 | 0.66 | 6.364 | 45.300 | 53 | 0.59 |
| | 318 | 7.097 | 47.402 | 49 | 0.73 | 8.649 | 46.939 | 52 | 0.59 |
| WL- γ -APS/MG | 298 | 6.397 | 59.574 | 50 | 0.57 | 6.181 | 60.638 | 52 | 0.67 |
| | 308 | 6.364 | 62.494 | 48 | 0.57 | 6.479 | 61.336 | 55 | 0.68 |
| | 318 | 6.650 | 63.184 | 48 | 0.59 | 6.779 | 63.999 | 50 | 0.69 |

The determination of the number of ions that interact with one receptor site offers reliable information complementing the conclusions for adsorption phenomena obtained from the isothermal adsorption study. If the number of the bonded/complexed ions/oxyanions per site is lower than 1, the ions interact with at least two receptor sites (multi-link). Opposite, if the n is higher than 1, the receptor site is occupied minimum by one ion (Sellaoui et al. 2017b, a). For all of the investigated single-compound systems (adsorption of Cd^{2+} , Ni^{2+} , $\text{HCrO}_4^-/\text{CrO}_4^{2-}$ and $\text{H}_2\text{PO}_4^-/\text{HPO}_4^{2-}$ on WL based adsorbents), the lowest values of the n are obtained at 298 K. It confirms that the main mechanism of the Cd^{2+} and Ni^{2+} ions adsorption occurs via exchange of metal ions $\text{Cd}^{2+}/\text{Ni}^{2+}$ with H^+ ions at the surface hydroxyl groups $-\text{FeOH}$ (receptor site)

producing $\text{Cd}^{2+}/\text{Ni}^{2+}(\text{OH})^+$ ions that are bonded with another MG modified WL receptor site. Also, electrostatic interactions of ion positive charge with electron pair of hydroxyl groups could be of appropriate significance. By changing the adsorption operational conditions (increasing temperature) the values of the n increase as well. For the Cd^{2+} ions adsorption on both WL-MG and WL- γ -APS/MG adsorbents the highest values of n (higher than 1) are obtained at 318 K. This indicates appropriate change of metal binding mechanism, *i.e.* higher number of ions per one site, with concomitant increase of adsorption capacity (Table 2). Opposite is found for Ni^{2+} ions adsorption on WL-MG adsorbent where the highest values of n is obtained at 298 K. Lower values of n parameters are found for the $\text{HCrO}_4^-/\text{CrO}_4^{2-}$ and $\text{H}_2\text{PO}_4^-/\text{HPO}_4^{2-}$ ions (Table 5) indicating different adsorption mechanism in relation to cations. The n values in the range 0.57-0.73 for $\text{HCrO}_4^-/\text{CrO}_4^{2-}$ and 0.59-0.69 for $\text{H}_2\text{PO}_4^-/\text{HPO}_4^{2-}$ indicates that main mechanism represent interaction one ion per two active surface sites which is in good accordance with creation of bidentate mononuclear and binuclear surface complexes of both ions (Zach-Maor et al. 2011; Johnston and Chrysochoou 2014). The parameter n also increases with temperature increase.

Conclusion

Magnetite modified porous wollastonite-based ceramics were synthesized using ultra-fine PMMA as a pore-forming agent in order to obtain hybrid adsorbents with high adsorption performances for heavy metals and oxyanions. FTIR, Raman, XRD and Mössbauer measurements confirmed wollastonite and larnite phases at pure WL support and successfulness of magnetite precipitation. SEM analysis confirmed macro and micro porosity of pure WL support and formation of MG aggregates on WL. Synthesized MG-modified WL-based sorbent was used for Cd^{2+} , Ni^{2+} , $\text{HCrO}_4^-/\text{CrO}_4^{2-}$ and $\text{H}_2\text{PO}_4^-/\text{HPO}_4^{2-}$ ions removal. Results showed that pH is an important parameter that controls the effectiveness of pollutant removal.

The quality of the isotherm modeling of adsorption data was estimated by the correlation coefficients. The best adsorption model was found to be the Langmuir isotherm. The kinetic data of the sorption were well fitted with the pseudo-second-order kinetic model. A significantly higher second-order rate constant of Cd^{2+} , Ni^{2+} , $\text{HCrO}_4^-/\text{CrO}_4^{2-}$ and $\text{H}_2\text{PO}_4^-/\text{HPO}_4^{2-}$ ions adsorption was obtained using WL- γ -APS/MG as adsorbent. Higher activation energies were obtained for oxyanion adsorption.

Statistical physic theory was used for interpretation of single adsorption isotherms and adsorption phenomena. The absorption parameters in a single-compound system deduced by the monolayer model with one energy confirmed that the adsorption of Cd^{2+} and Ni^{2+} ions occurred via mostly one ion with two receptor sites interactions. For the $\text{HCrO}_4^-/\text{CrO}_4^{2-}$ and $\text{H}_2\text{PO}_4^-/\text{HPO}_4^{2-}$ ions adsorption, the statistical physic model confirmed that multiple adsorption mechanisms electrostatic interaction/complexation occurred.

Acknowledgement

This research was performed within the projects OI 172057, OI 171001, and 176018, funded by the Ministry of Education, Science and Technological Development of the Republic of Serbia, and bilateral cooperation between Serbia and France, No. 4510339/2016/09/03 “Intelligent eco-nanomaterials and nanocomposites”. The work was supported in part by the National Science Foundation, North Carolina State University (Project No. HRD-1345219 and DMR-1523617) and the National Aeronautics and Space Administration project (NASA: NNX09AV07A). The authors are grateful to Dr. Miodrag Mitrić for XRD measurements.

References

- Abdel-Halim ES, Al-Deyab SS (2011) Removal of heavy metals from their aqueous solutions through adsorption onto natural polymers. *Carbohydr Polym* 84:454–458. doi: 10.1016/j.carbpol.2010.12.001
- Ahmed MA, Ali SM, El-Dek SI, Galal A (2013) Magnetite–hematite nanoparticles prepared by green methods for heavy metal ions removal from water. *Mater Sci Eng B* 178:744–751. doi: 10.1016/j.mseb.2013.03.011
- Bizerea Spiridon O, Pitulice L (2014) Phenol removal from wastewater by adsorption on zeolitic composite. *Environ Sci Pollut Res* (2013) 20:6367–6381. doi: 10.1007/s11356-013-1625-x
- Boehm HP (1994) Some aspects of the surface chemistry of carbon blacks and other carbons. *Carbon N Y* 32:759–769
- Brand R (2008) WinNormos Mössbauer fitting program
- Budimirović D, Veličković ZS, Djokić VR, et al (2017) Efficient As(V) removal by α -FeOOH and α -FeOOH/ α -MnO₂ embedded PEG-6-arm functionalized multiwall carbon nanotubes. *Chem Eng Res Des* 119:75–86. doi: 10.1016/j.cherd.2017.01.010
- Buzatu A, Buzgar N (2010) The Raman study of single-chain silicates. *Analele Stiint ale Univ "Al I Cuza" din Iasi*, Geol 56:107–125. doi: 10.13140/2.1.4600.9288
- Capretta A, Maharajh RB, Bell RA (1995) Synthesis and characterization of cyclomaltoheptaose-based metal chelants as probes for intestinal permeability. *Carbohydr Res* 267:49–63. doi: 10.1016/0008-6215(94)00289-R
- Carvalho MD, Henriques F, Ferreira LP, et al (2013) Iron oxide nanoparticles: The influence of synthesis method and size on composition and magnetic properties. *J Solid State Chem* 201:144–152. doi: 10.1016/j.jssc.2013.02.024
- Chen Q, Hills CD, Yuan M, et al (2008) Characterization of carbonated tricalcium silicate and its sorption capacity for heavy metals: A micron-scale composite adsorbent of active silicate gel and calcite. *J Hazard Mater* 153:775–783. doi: 10.1016/j.jhazmat.2007.09.023

- Costa GM, De Grave E, Vandenberghe RE (1998) Mössbauer studies of magnetite and Al-substituted maghemites. *Hyperfine Interact* 117:207–243. doi: 10.1023/A:1012691209853
- D'Halluin M, Rull-Barrull J, Bretel G, et al (2017) Chemically modified cellulose filter paper for heavy metal remediation in water. *ACS Sustain Chem Eng* 5:1965–1973. doi: 10.1021/acssuschemeng.6b02768
- da Costa GM (1995) Influence of Nonstoichiometry and the Presence of Maghemite on the Mössbauer Spectrum of Magnetite†. *Clays Clay Miner* 43:656–668. doi: 10.1346/CCMN.1995.0430602
- de Faria DLA, Venâncio Silva S, de Oliveira MT (1997) Raman microspectroscopy of some iron oxides and oxyhydroxides. *J Raman Spectrosc* 28:873–878. doi: 10.1002/(SICI)1097-4555(199711)28:11<873::AID-JRS177>3.0.CO;2-B
- Dézsi I, Fetzer C, Gombkötő Á, et al (2008) Phase transition in nanomagnetite. *J Appl Phys* 103:104312. doi: 10.1063/1.2937252
- Ding H, Lu SC, Du GX (2011) Surface modification of wollastonite by the mechano-activated method and its properties. *Int J Miner Metall Mater* 18:83–88. doi: 10.1007/s12613-011-0404-2
- Dowty E, Lindsley DH (1973) Mössbauer spectra of synthetic Ca-Fe pyroxenoids and lunar pyroxferroite. *Contrib to Mineral Petrol* 48:229–232. doi: 10.1007/BF00383358
- Drah A, Tomić NZ, Veličić Z, et al (2017) Highly ordered macroporous γ -alumina prepared by a modified sol-gel method with a PMMA microsphere template for enhanced Pb^{2+} , Ni^{2+} and Cd^{2+} removal. *Ceram Int* 43:13817–13827. doi: 10.1016/j.ceramint.2017.07.102
- Dyar MD, Agresti DG, Schaefer MW, et al (2006) Mössbauer Spectroscopy of Earth and Planetary Materials. *Annu Rev Earth Planet Sci* 34:83–125. doi: 10.1146/annurev.earth.34.031405.125049
- Ebbert C, Grundmeier G, Buitkamp N, et al (2014) Toward a microscopic understanding of the calcium–silicate–hydrates/water interface. *Appl Surf Sci* 290:207–214. doi: 10.1016/j.apsusc.2013.11.045
- EPA (2014) United State Environmental Protection Agency
- Fock J, Bogart LK, González-Alonso D, et al (2017) On the ‘centre of gravity’ method for measuring the composition of magnetite/maghemite mixtures, or the stoichiometry of magnetite-maghemite solid solutions, via ^{57}Fe Mössbauer spectroscopy. *J Phys D Appl Phys* 50:265005. doi: 10.1088/1361-6463/aa73fa
- Gorski CA, Scherer MM (2010) Determination of nanoparticulate magnetite stoichiometry by Mössbauer spectroscopy, acidic dissolution, and powder X-ray diffraction: A critical review. *Am Mineral* 95:1017–1026. doi: 10.2138/am.2010.3435
- Gustafsson JP (2011) Visual MINTEQ. 3.0, beta

- 1
- 2
- 3
- 4 Han Q, Chen L, Li W, et al (2018) Self-assembled three-dimensional double network graphene
- 5 oxide/polyacrylic acid hybrid aerogel for removal of Cu²⁺ from aqueous solution. *Environ*
- 6 *Sci Pollut Res* 25:34438–34447. doi: 10.1007/s11356-018-3409-9
- 7
- 8
- 9 Haring MM (1942) The Theory of Rate Processes (Glasstone, Samuel; Laidler, Keith J.; Eyring,
- 10 Henry). *J Chem Educ* 19:249. doi: 10.1021/ed019p249.1
- 11
- 12 Huang X, Zhan X, Wen C, et al (2017) Amino-functionalized magnetic bacterial
- 13 cellulose/activated carbon composite for Pb²⁺ and methyl orange sorption from aqueous
- 14 solution. *J Mater Sci Technol*. doi: 10.1016/j.jmst.2017.03.013
- 15
- 16
- 17 Iannazzo D, Pistone A, Ziccarelli I, et al (2017) Removal of heavy metal ions from wastewaters
- 18 using dendrimer-functionalized multi-walled carbon nanotubes. *Environ Sci Pollut Res*
- 19 24:14735–14747. doi: 10.1007/s11356-017-9086-2
- 20
- 21 Johnston CP, Chrysochoou M (2014) Mechanisms of chromate adsorption on hematite. *Geochim*
- 22 *Cosmochim Acta* 138:146–175
- 23
- 24 Joos A, Rümenapp C, Wagner FE, Gleich B (2016) Characterisation of iron oxide nanoparticles
- 25 by Mössbauer spectroscopy at ambient temperature. *J Magn Magn Mater* 399:123–129. doi:
- 26 10.1016/j.jmmm.2015.09.060
- 27
- 28
- 29 Kalantari K, Ahmad MB, Masoumi HRF, et al (2014) Rapid adsorption of heavy metals by
- 30 Fe₃O₄/talc nanocomposite and optimization study using response surface methodology. *Int J*
- 31 *Mol Sci* 15:12913–12927. doi: 10.3390/ijms150712913
- 32
- 33
- 34 Kalska-Szostko B, Satuła D, Olszewski W (2015) Mössbauer spectroscopy studies of the
- 35 magnetic properties of ferrite nanoparticles. *Curr Appl Phys* 15:226–231. doi:
- 36 10.1016/j.cap.2014.12.011
- 37
- 38 Karnib M, Kabbani A, Holail H, Olama Z (2014) Heavy metals removal using activated carbon,
- 39 silica and silica activated carbon composite. *Energy Procedia* 50:113–120. doi:
- 40 10.1016/j.egypro.2014.06.014
- 41
- 42
- 43 Karthikeyan T, Rajgopal S, Miranda LR (2005) Chromium(VI) adsorption from aqueous
- 44 solution by Hevea Brasilinesis sawdust activated carbon. *J Hazard Mater* 124:192–199. doi:
- 45 10.1016/j.jhazmat.2005.05.003
- 46
- 47
- 48 Khalil MI (2015) Co-precipitation in aqueous solution synthesis of magnetite nanoparticles using
- 49 iron(III) salts as precursors. *Arab J Chem* 8:279–284. doi: 10.1016/j.arabjc.2015.02.008
- 50
- 51
- 52 Kumari M, Pittman CU, Mohan D (2015) Heavy metals [chromium(VI) and lead(II)] removal
- 53 from water using mesoporous magnetite (Fe₃O₄) nanospheres. *J Colloid Interface Sci*
- 54 442:120–132. doi: 10.1016/j.jcis.2014.09.012
- 55
- 56
- 57 Kündig W, Steven Hargrove R (1969) Electron hopping in magnetite. *Solid State Commun*
- 58 7:223–227. doi: 10.1016/0038-1098(69)90729-7
- 59
- 60
- 61 Li Y-S, Church JS, Woodhead AL (2012) Infrared and Raman spectroscopic studies on iron
- 62 oxide magnetic nano-particles and their surface modifications. *J Magn Magn Mater*
- 63
- 64
- 65

324:1543–1550. doi: 10.1016/j.jmmm.2011.11.065

- Lin S, Lian C, Xu M, et al (2017) Study on competitive adsorption mechanism among oxyacid-type heavy metals in co-existing system : Removal of aqueous As(V), Cr(III) and As (III) using magnetic iron oxide nanoparticles (MIONPs) as adsorbents. 422:675–681. doi: 10.1016/j.apsusc.2017.06.079
- Liu C-H, Chuang Y-H, Chen T-Y, et al (2015) Mechanism of arsenic adsorption on magnetite nanoparticles from water: Thermodynamic and spectroscopic studies. Environ Sci Technol 49:7726–7734. doi: 10.1021/acs.est.5b00381
- March J (1985) Advanced organic chemistry: Reaction, mechanisms and structure. John Wiley & Sons Inc., New York
- Markovski JS, Đokić V, Milosavljević M, et al (2014a) Ultrasonic assisted arsenate adsorption on solvothermally synthesized calcite modified by goethite, α -MnO₂ and goethite/ α -MnO₂. Ultrason Sonochem 21:790–801. doi: 10.1016/j.ultsonch.2013.10.006
- Markovski JS, Marković DD, Đokić VR, et al (2014b) Arsenate adsorption on waste eggshell modified by goethite, α -MnO₂ and goethite/ α -MnO₂. Chem Eng J 237:430–442. doi: 10.1016/j.cej.2013.10.031
- Martin S, Griswold W (2009) Human health effects of heavy metals. Cent. Hazard. Subst. Res. Environmental Sci. Technol. Briefs Citizens 1–6
- Mezenner NY, Bensmaili A (2009) Kinetics and thermodynamic study of phosphate adsorption on iron hydroxide-eggshell waste. Chem Eng J 147:87–96. doi: 10.1016/j.cej.2008.06.024
- Murad E, Wagner U (1998) Clays and clay minerals: The firing process. Hyperfine Interact 117:337–356. doi: 10.1023/A:1012683008035
- Obradović N, Filipović S, Marković S, et al (2017a) Influence of different pore-forming agents on wollastonite microstructures and adsorption capacities. Ceram Int 43:7461–7468. doi: 10.1016/j.ceramint.2017.03.021
- Obradović N, Filipović S, Rusmirović J, et al (2017b) Formation of porous wollastonite-based ceramics after sintering with yeast as the pore-forming agent. Sci Sinter 49:. doi: 10.2298/SOS1703235O
- Oshtrakh MI, Ushakov MV, Šepelák V, et al (2016) Study of iron oxide nanoparticles using Mössbauer spectroscopy with a high velocity resolution. Spectrochim Acta Part A Mol Biomol Spectrosc 152:666–679. doi: 10.1016/j.saa.2015.06.017
- Osticioli I, Mendes NFC, Nevin A, et al (2009) Analysis of natural and artificial ultramarine blue pigments using laser induced breakdown and pulsed Raman spectroscopy, statistical analysis and light microscopy. Spectrochim Acta Part A Mol Biomol Spectrosc 73:525–531. doi: 10.1016/j.saa.2008.11.028
- Ovsyannikov S V., Shchennikov V V., Shvetsova MA, et al (2010) Tuning of the stoichiometry of Fe_{1-x}O wüstite by compression wüstite by compression. Phys Rev B 81:060101. doi:

1
2
3
4 10.1103/PhysRevB.81.060101
5

6 Paul D (2017) Research on heavy metal pollution of river Ganga: A review. *Ann Agrar Sci*
7 15:278–286. doi: 10.1016/j.aasci.2017.04.001
8

9
10 Petrova TM, Fachikov L, Hristov J (2011) The magnetite as adsorbent for some hazardous
11 species from aqueous solution: A review. *Int Rev Chem Eng Int Rev Chem Eng* 3:134–152
12

13 Qi Z, Joshi TP, Liu R, et al (2017) Synthesis of Ce(III)-doped Fe₃O₄ magnetic particles for
14 efficient removal of antimony from aqueous solution. *J Hazard Mater* 329:193–204. doi:
15 10.1016/j.jhazmat.2017.01.007
16

17 Qiu H, Lv L, Pan B, et al (2009) Critical review in adsorption kinetic models. *J Zhejiang Univ*
18 *Sci A* 10:716–724. doi: 10.1631/jzus.A0820524
19

20
21 Rajput S, Pittman CU, Mohan D (2016) Magnetic magnetite (Fe₃O₄) nanoparticle synthesis and
22 applications for lead (Pb²⁺) and chromium (Cr⁶⁺) removal from water. *J Colloid Interface*
23 *Sci* 468:334–346. doi: 10.1016/j.jcis.2015.12.008
24

25 Razzaque MS (2011) Phosphate toxicity: new insights into an old problem. *Clin Sci* 120:91–97.
26 doi: 10.1042/CS20100377
27

28 Ricciardi P, Colomban P, Tournié A, Milande V (2009) Nondestructive on-site identification of
29 ancient glasses: genuine artefacts, embellished pieces or forgeries? *J Raman Spectrosc*
30 40:604–617. doi: 10.1002/jrs.2165
31

32
33 Richet P, Mysen BO, Ingrin J (1998) High-temperature X-ray diffraction and Raman
34 spectroscopy of diopside and pseudowollastonite. *Phys Chem Miner* 25:401–414. doi:
35 10.1007/s002690050130
36

37 Roggwiller P, Kundig W (1973) Mössbauer spectra of superparamagnetic Fe₃O₄. *Differentiation*
38 12:901–903
39

40
41 Rouquerol F, Rouquerol J, Sing, Kenneth (1999) Adsorption by powders and porous solids:
42 Principles, methodology and application. Academic Press, USA
43

44 Rout PR, Bhunia P, Dash RR (2015) Effective utilization of a sponge iron industry by-product
45 for phosphate removal from aqueous solution: A statistical and kinetic modelling approach.
46 *J Taiwan Inst Chem Eng* 46:98–108. doi: 10.1016/j.jtice.2014.09.006
47

48
49 Rout PR, Dash RR, Bhunia P (2016) Nutrient removal from binary aqueous phase by dolochar :
50 Highlighting optimization, single and binary adsorption isotherms and nutrient release.
51 *Process Saf Environ Prot* 100:91–107. doi: 10.1016/j.psep.2016.01.001
52

53 Sarin VK, Kent SBH, Tam JP, Merrifield RB (1981) Quantitative monitoring of solid-phase
54 peptide synthesis by the ninhydrin reaction. *Anal Biochem* 117:147–157. doi:
55 10.1016/0003-2697(81)90704-1
56

57
58 Sellaoui L, Bouzid M, Duclaux L, et al (2016a) Binary adsorption isotherms of two ionic liquids
59 and ibuprofen on an activated carbon cloth: simulation and interpretations using a statistical
60
61
62
63
64
65

- and COSMO-RS models. RSC Adv 6:67701–67714. doi: 10.1039/C6RA03405E
- Sellaoui L, Dotto GL, Goncalves JO, et al (2016b) Equilibrium modeling of single and binary adsorption of Food Yellow 4 and Food Blue 2 on modified chitosan using a statistical physics theory: new microscopic interpretations. J Mol Liq 222:151–158. doi: 10.1016/j.molliq.2016.07.005
- Sellaoui L, Dotto GL, Lamine A Ben, Erto A (2017a) Interpretation of single and competitive adsorption of cadmium and zinc on activated carbon using monolayer and exclusive extended monolayer models. Environ Sci Pollut Res 24:19902–19908. doi: 10.1007/s11356-017-9562-8
- Sellaoui L, Edi Soetaredjo F, Ismadji S, et al (2017b) New insights into single-compound and binary adsorption of copper and lead ions on treated sea mango shell: Experimental and theoretical studies. Phys Chem Chem Phys 19:25927–25937. doi: 10.1039/c7cp03770h
- Sharma YC (2001) Adsorption of Cr(VI) onto wollastonite: Effect of pH. Indian J Chem Technol 8:186–190
- Sharma YC, Gupta GS, Prasad G, Rupainwar DC (1990a) Use of wollastonite in the removal of Ni(II) from aqueous solutions. Water Air Soil Pollut 49:69–79. doi: 10.1007/BF00279511
- Sharma YC, Prasad G, Rupainwar DI (1990b) Adsorption for removal of Cd(II) from effluents. Int J Environ Stud 36:315–320. doi: 10.1080/00207239008710609
- Sharma YC, Uma, Srivastava V, et al (2007) Reclamation of Cr(VI) rich water and wastewater by wollastonite. Chem Eng J 127:151–156. doi: 10.1016/j.cej.2006.09.012
- Shim SE, Kim K, Oh S, Choe S (2004) Preparation of ultra fine poly(methyl methacrylate) microspheres in methanol-enriched aqueous medium. Macromol Res 12:240–245. doi: 10.1007/BF03218394
- Sokol E V., Seryotkin Y V., Kokh SN, et al (2015) Flamite, $(\text{Ca,Na,K})_2(\text{Si,P})\text{O}_4$, a new mineral from ultrahightemperature combustion metamorphic rocks, Hatrurim Basin, Negev Desert, Israel. Mineral Mag 79:583–596. doi: 10.1180/minmag.2015.079.3.05
- Sreekanth Chakradhar RP, Nagabhushana BM, Chandrappa GT, et al (2006) Solution combustion derived nanocrystalline macroporous wollastonite ceramics. Mater Chem Phys 95:169–175. doi: 10.1016/j.matchemphys.2005.06.002
- Stevens JG, Khasanov AM, Miller JW, et al (2005) Mössbauer Mineral Handbook. The University of North Carolina at Asheville
- Suzdalev IP, Maksimov Y V., Buravtsev VN, et al (2012) Magnetic properties of monodisperse nanomagnetite. Russ J Phys Chem B 6:163–168. doi: 10.1134/S1990793112010228
- Swamy V, Dubrovinsky LS, Tutti F (1997) High-temperature raman spectra and thermal expansion of wollastonite. J Am Ceram Soc 80:2237–2247. doi: 10.1111/j.1151-2916.1997.tb03113.x

- 1
- 2
- 3
- 4 Taleb K, Markovski J, Milosavljević M, et al (2015) Efficient arsenic removal by cross-linked
- 5 macroporous polymer impregnated with hydrous iron oxide: Material performance. *Chem*
- 6 *Eng J* 279:.. doi: 10.1016/j.cej.2015.04.147
- 7
- 8
- 9 Taleb K, Markovski J, Veličković Z, et al (2016a) Arsenic removal by magnetite-loaded amino
- 10 modified nano/microcellulose adsorbents: Effect of functionalization and media size. *Arab J*
- 11 *Chem*. doi: 10.1016/j.arabjc.2016.08.006
- 12
- 13 Taleb KA, Rusmirović JD, Rančić MP, et al (2016b) Efficient pollutants removal by amino-
- 14 modified nanocellulose impregnated with iron oxide. *J Serbian Chem Soc* 81:.. doi:
- 15 10.2298/JSC160529063T
- 16
- 17
- 18 Tejedor-Tejedor MI, Anderson MA (1990) The protonation of phosphate on the surface of
- 19 goethite as studied by CIR-FTIR and electrophoretic mobility. *Langmuir* 6:602–611. doi:
- 20 10.1021/la00093a015
- 21
- 22 Veličković Z, Vuković GD, Marinković AD, et al (2012) Adsorption of arsenate on iron(III)
- 23 oxide coated ethylenediamine functionalized multiwall carbon nanotubes. *Chem Eng J* 181–
- 24 182:174–181. doi: 10.1016/j.cej.2011.11.052
- 25
- 26
- 27 Vuković GD, Marinković AD, Čolić M, et al (2010) Removal of cadmium from aqueous
- 28 solutions by oxidized and ethylenediamine-functionalized multi-walled carbon nanotubes.
- 29 *Chem Eng J* 157:238–248. doi: 10.1016/j.cej.2009.11.026
- 30
- 31
- 32 Vuković GD, Marinković AD, Škapin SD, et al (2011) Removal of lead from water by amino
- 33 modified multi-walled carbon nanotubes. *Chem Eng J* 173:855–865. doi:
- 34 10.1016/j.cej.2011.08.036
- 35
- 36
- 37 Wang X, Mao H, Huang W, et al (2011) Preparation of magnetic imprinted polymer particles via
- 38 microwave heating initiated polymerization for selective enrichment of 2-amino-4-
- 39 nitrophenol from aqueous solution. *Chem Eng J* 178:85–92. doi: 10.1016/j.cej.2011.10.015
- 40
- 41
- 42 Wang Y, Li B, Zhou Y, Jia D (2009) In situ mineralization of magnetite nanoparticles in
- 43 chitosan hydrogel. *Nanoscale Res Lett* 4:1041–1046. doi: 10.1007/s11671-009-9355-1
- 44
- 45
- 46
- 47 White SN (2009) Laser Raman spectroscopy as a technique for identification of seafloor
- 48 hydrothermal and cold seep minerals. *Chem Geol* 259:240–252. doi:
- 49 10.1016/j.chemgeo.2008.11.008
- 50
- 51
- 52 Zach-Maor A, Semiat R, Shemer H (2011) Adsorption–desorption mechanism of phosphate by
- 53 immobilized nano-sized magnetite layer: Interface and bulk interactions. *J Colloid Interface*
- 54 *Sci* 363:608–614. doi: 10.1016/j.jcis.2011.07.062
- 55
- 56
- 57
- 58 Zeng B, Yang L, Zheng W, et al (2017) Analysis of the formation process and performance of
- 59 magnetic Fe₃O₄@Poly(4-vinylpyridine) absorbent prepared by in-situ synthesis. *J Mater Sci*
- 60 *Technol* In press,.: doi: 10.1016/j.jmst.2017.07.007
- 61
- 62
- 63
- 64
- 65

Zhao J, Zhu YJ, Wu J, et al (2014) Chitosan-coated mesoporous microspheres of calcium silicate hydrate: Environmentally friendly synthesis and application as a highly efficient adsorbent for heavy metal ions. J Colloid Interface Sci 418:208–215. doi: 10.1016/j.jcis.2013.12.016

Figure Caption

Fig. 1. Schematic illustration of 1) direct attaching of MG spheres on WL and 2) attaching of MG spheres on amino/carboxylic acid functionalized WL

Fig. 2. ATR-FTIR spectra of modified wollastonite based adsorbents

Fig. 3. Raman spectra of W-MG and W- γ -APS/MG adsorbents

Fig. 4. XRD patterns of unmodified WL, WL/MG and WL- γ -APS/MG samples

Fig. 5. Room temperature Mössbauer spectrum of the a) WL/MG and b) WL- γ -APS/MG. (On each individual plot, experimental data are presented by solid circles and the fit is given by the red solid line. Vertical arrow denotes relative position of the lowermost peak with respect to the basal line. Red solid line in the lower part of the plot represents the error calculated as the difference (Th-Exp). a) The fitted lines of the Mössbauer subspectra are plotted above the main spectrum fit: D-subspectrum (blue) and B-subspectrum (orange). The largest value of the absolute difference is less than 0.2 %. b) The largest value of the absolute difference is less than 0.09 %.)

Fig. 6. The quadrupole splitting distribution $P(\Delta)$ of the WL- γ -APS/MG sample

Fig. 7. Black line – hyperfine magnetic field distribution $P(B_{\text{hf}})$ of the magnetic part of the WL/MG spectra. Red line - fit of the $P(B_{\text{hf}})$ distribution with five Gaussian (five blue lines)

Fig. 8. SEM micrograph of synthesized a) PMMA microsphere, b) unmodified WL, c) WL/MG and d) WL- γ -APS/MG

Fig. 9. EDS mapping of modified WL based adsorbents a) WL/MG and d) WL- γ -APS/MG



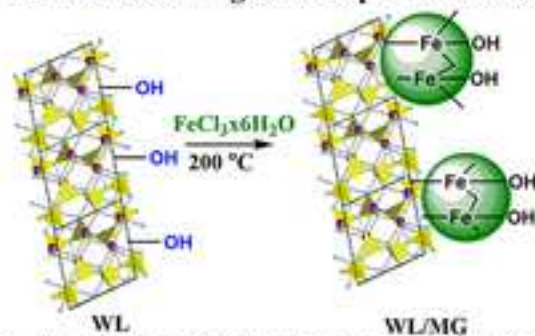
[Click here to access/download](#)

Supplementary Material

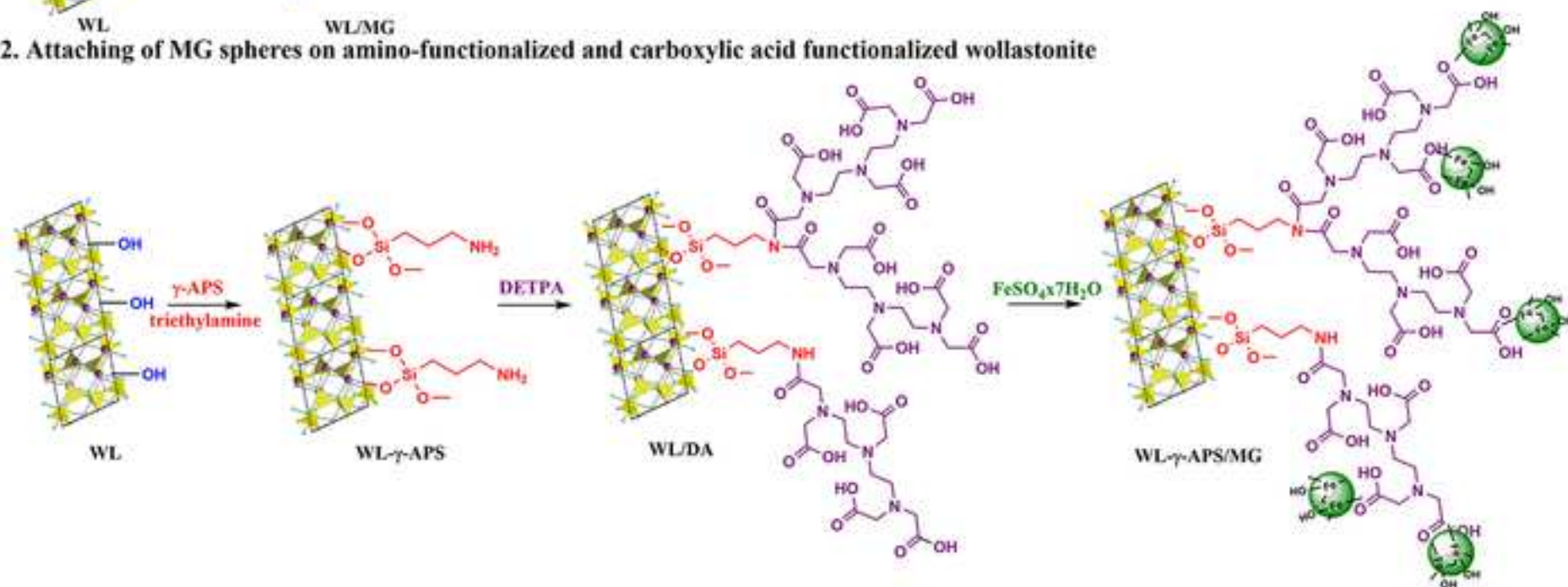
Rusmirovic et al _Supplementary material Revised.docx

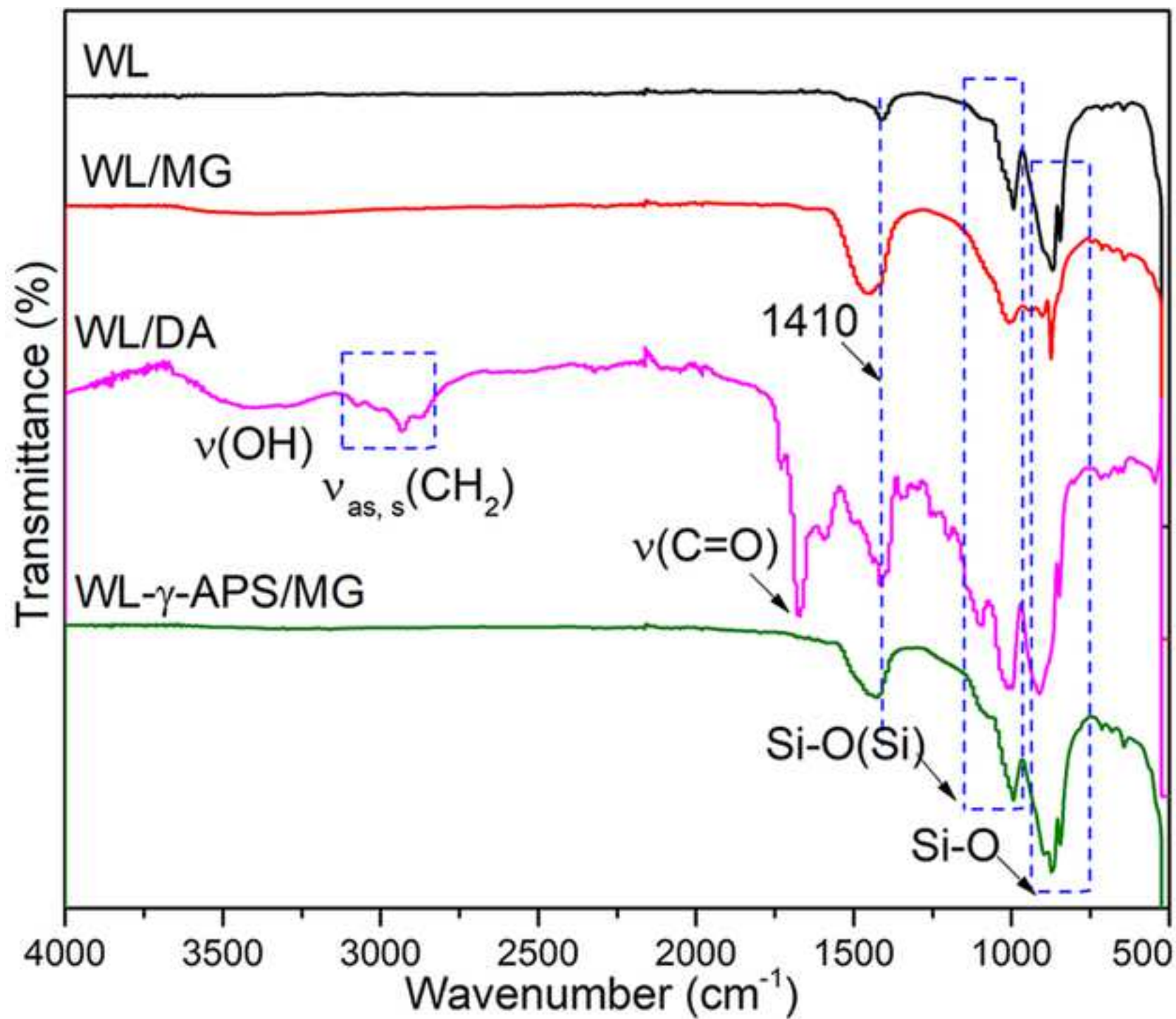


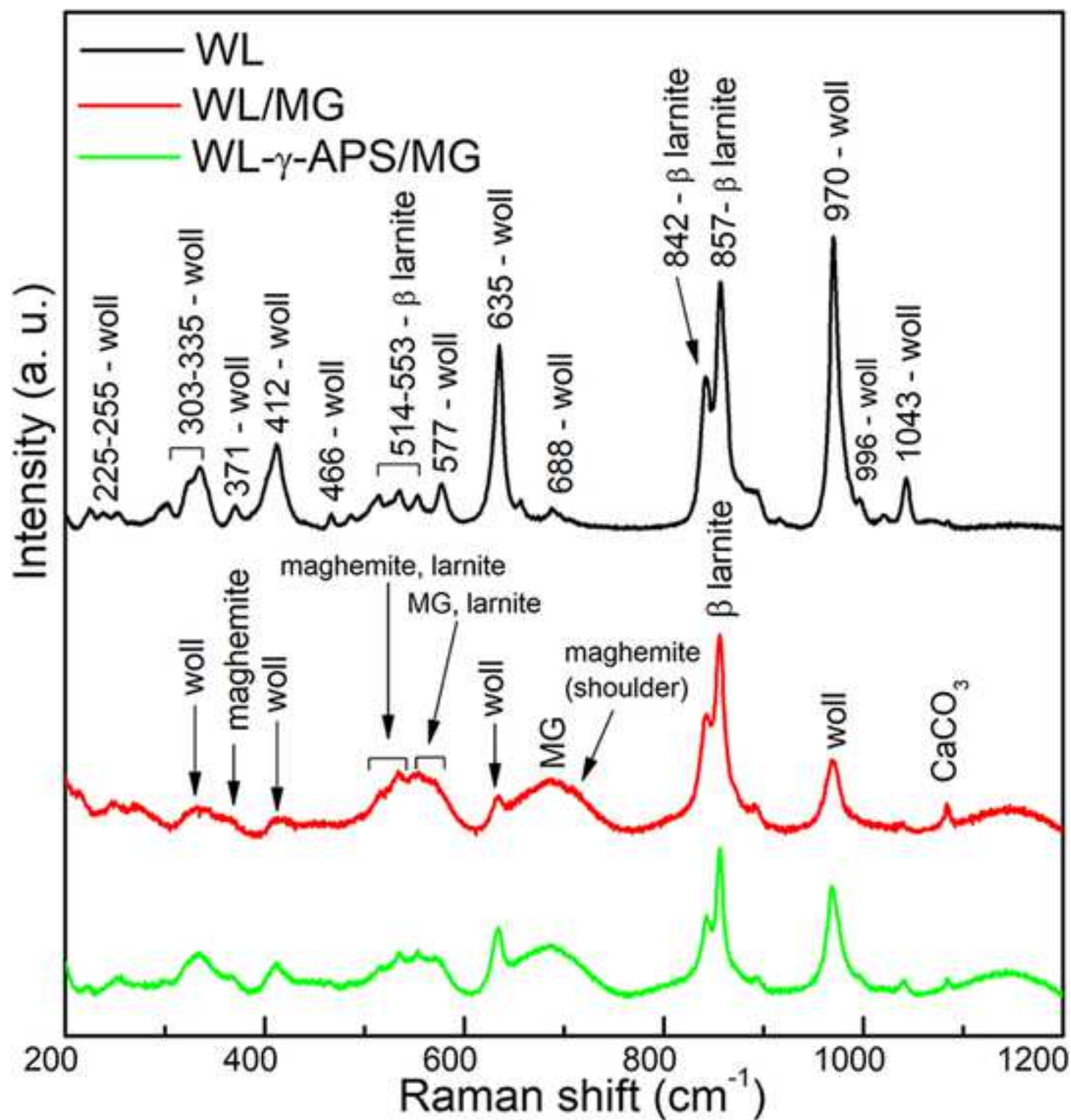
1. Direct attaching of MG spheres on wollastonite

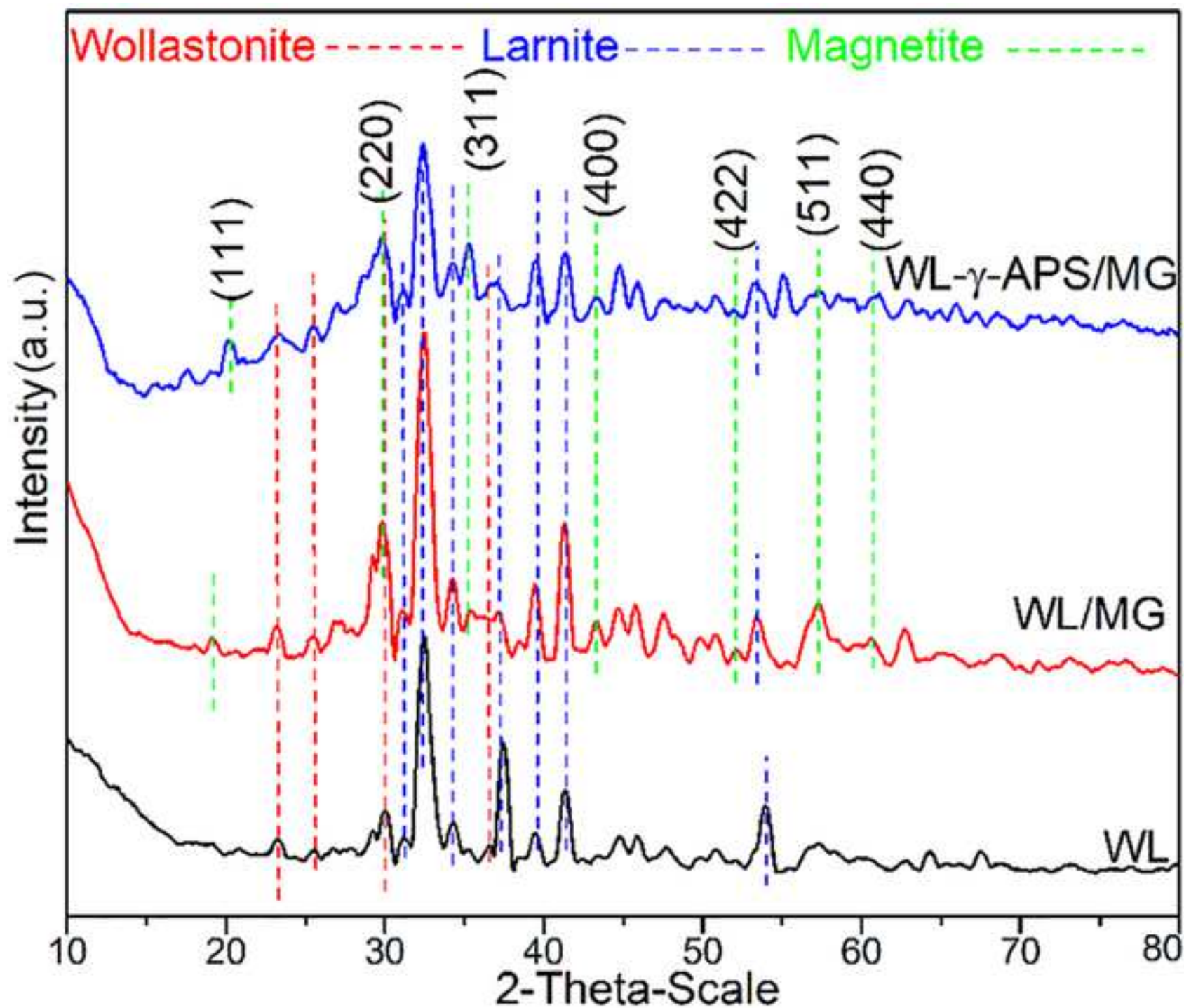


2. Attaching of MG spheres on amino-functionalized and carboxylic acid functionalized wollastonite









Relative transmission

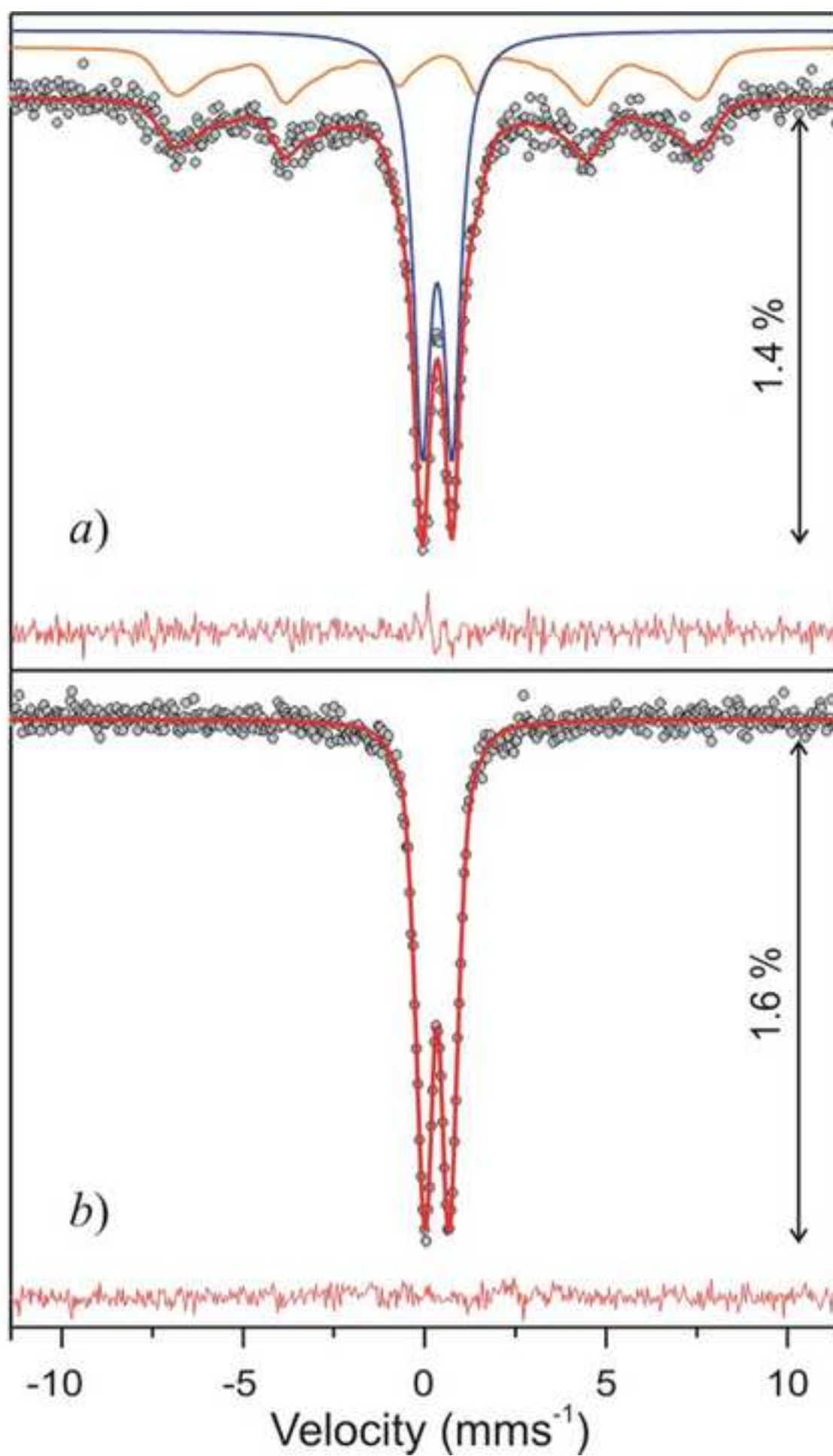


Figure6

[Click here to access/download;Figure;Fig 6.jpg](#) 

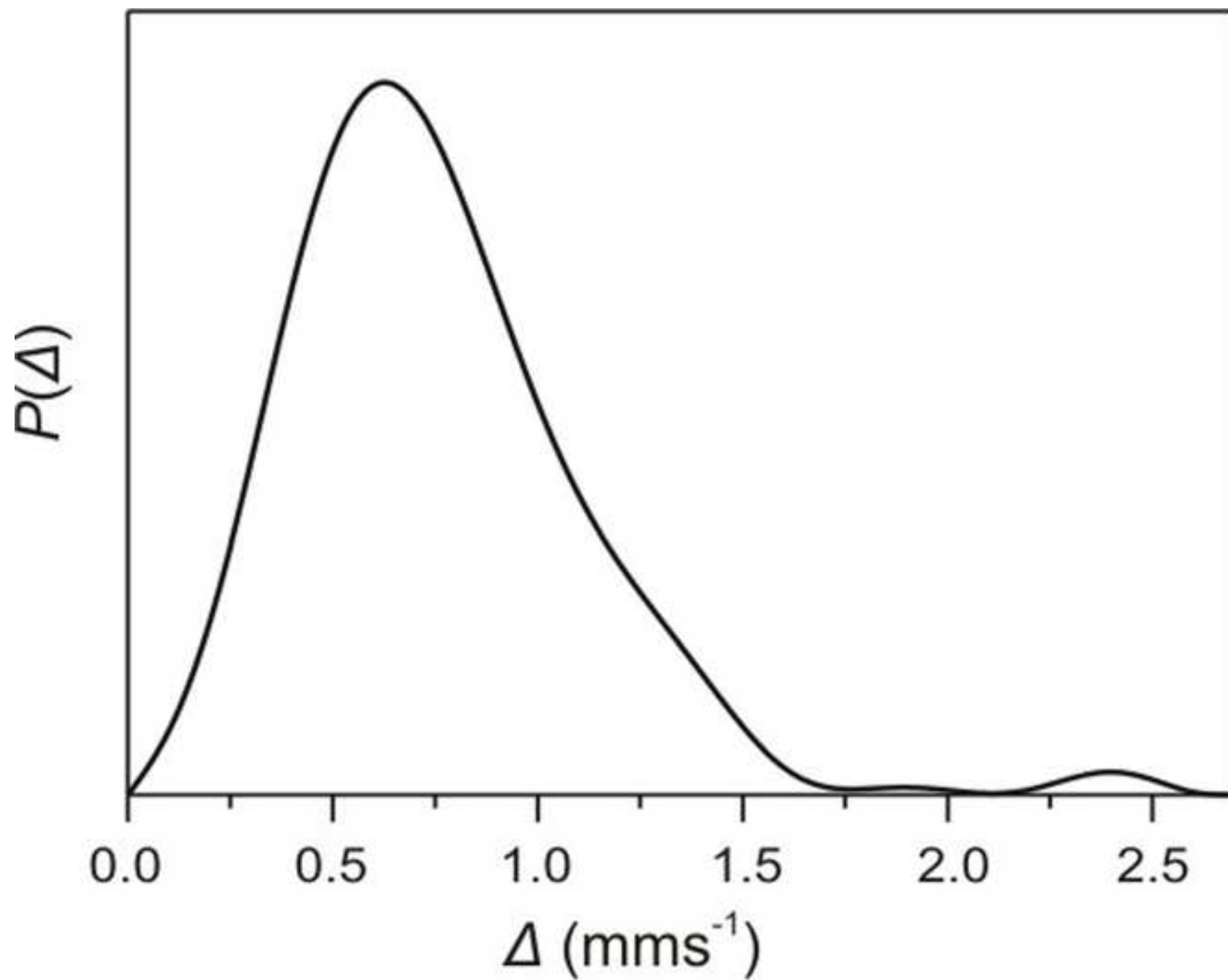
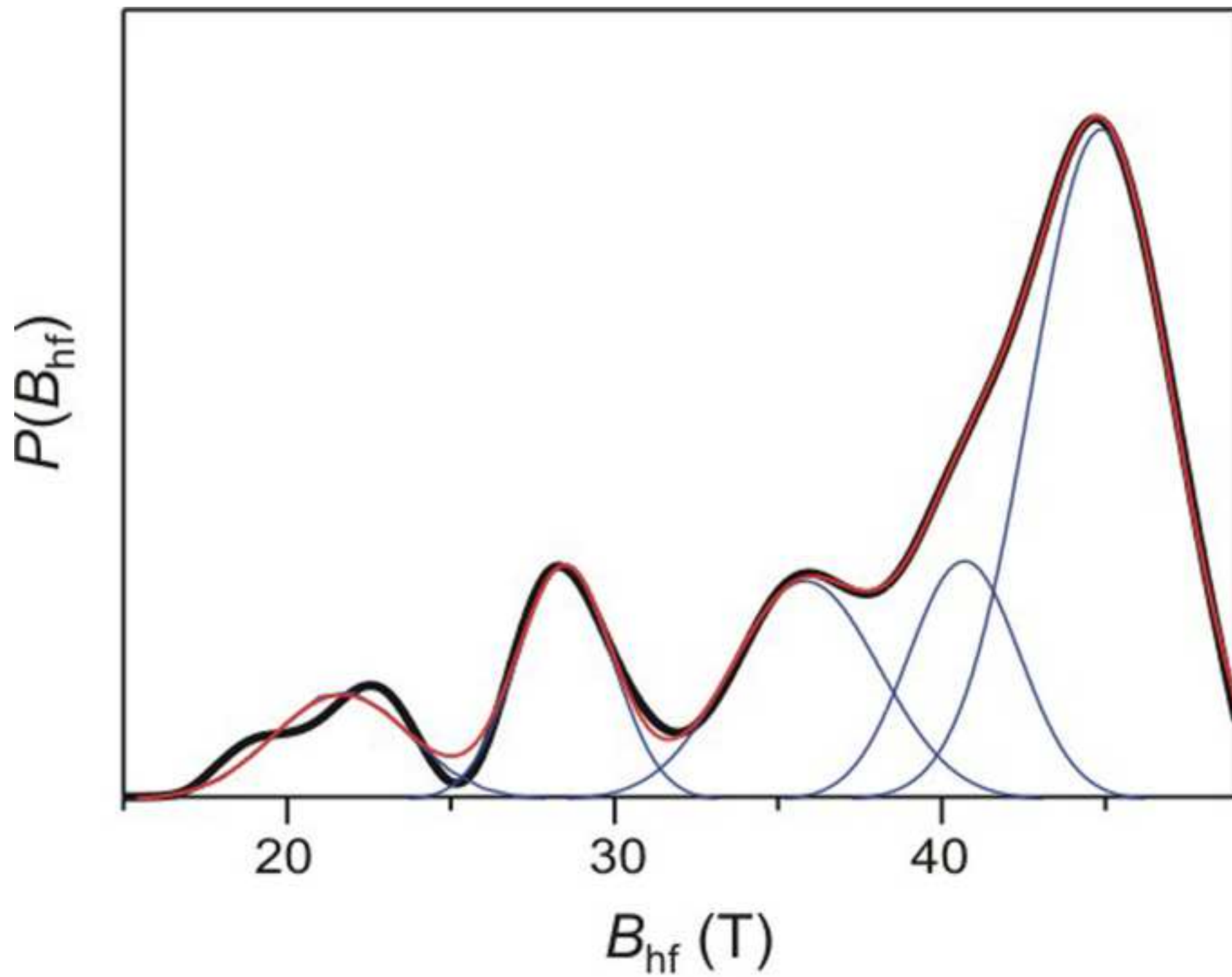
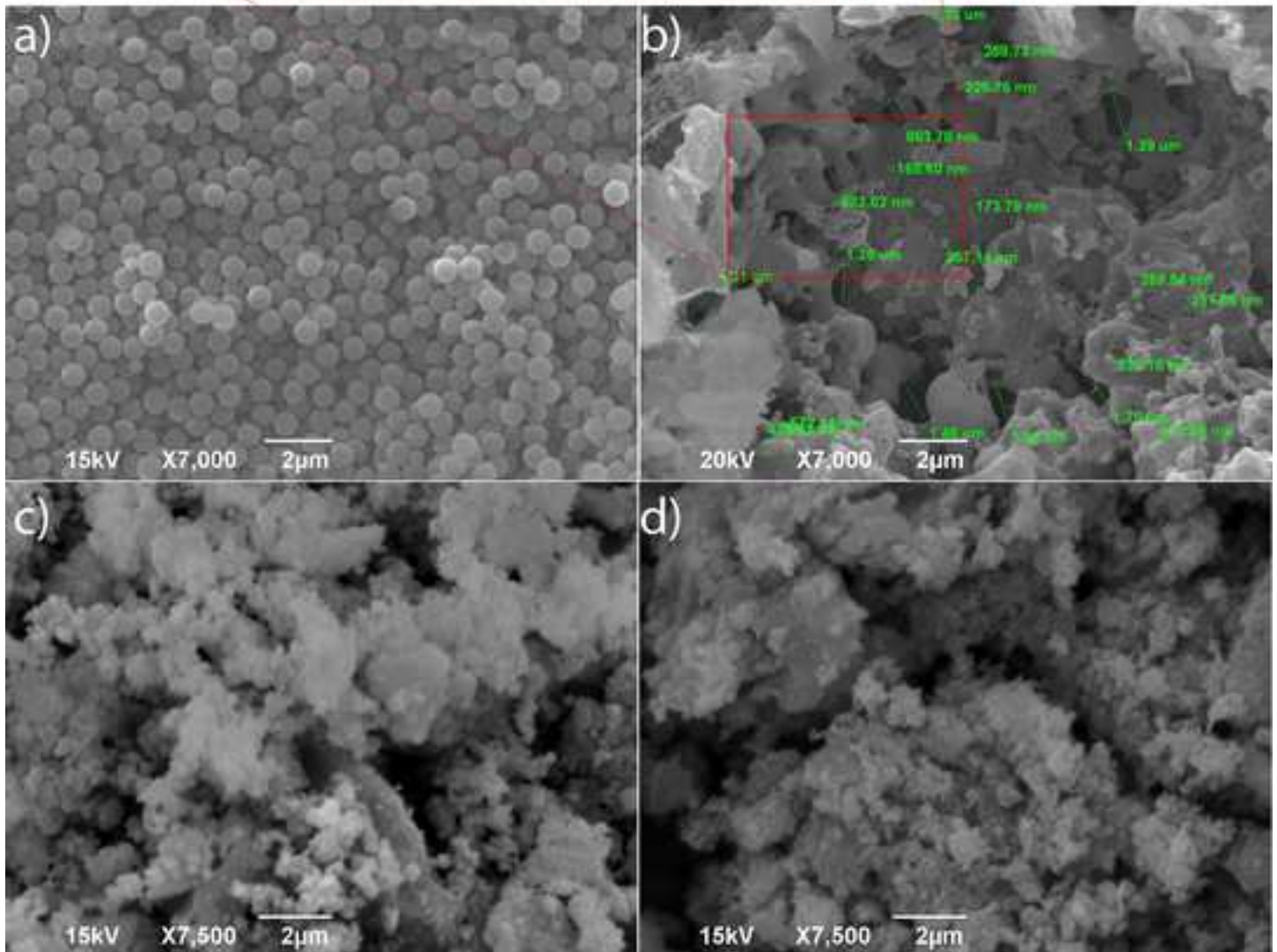
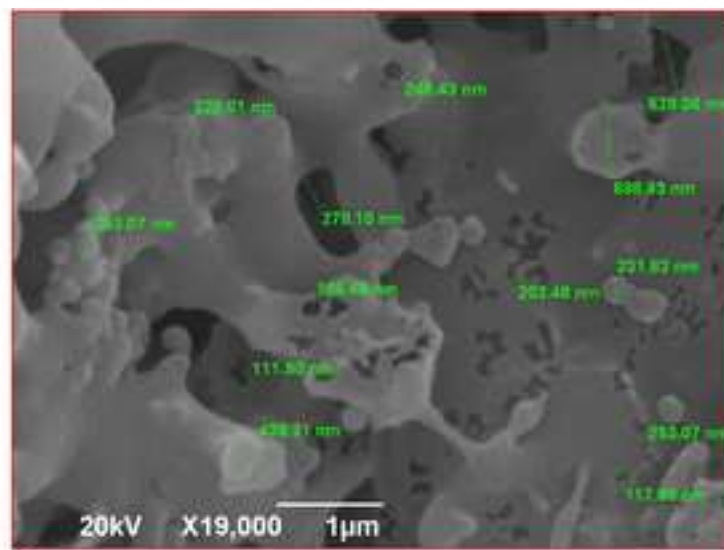
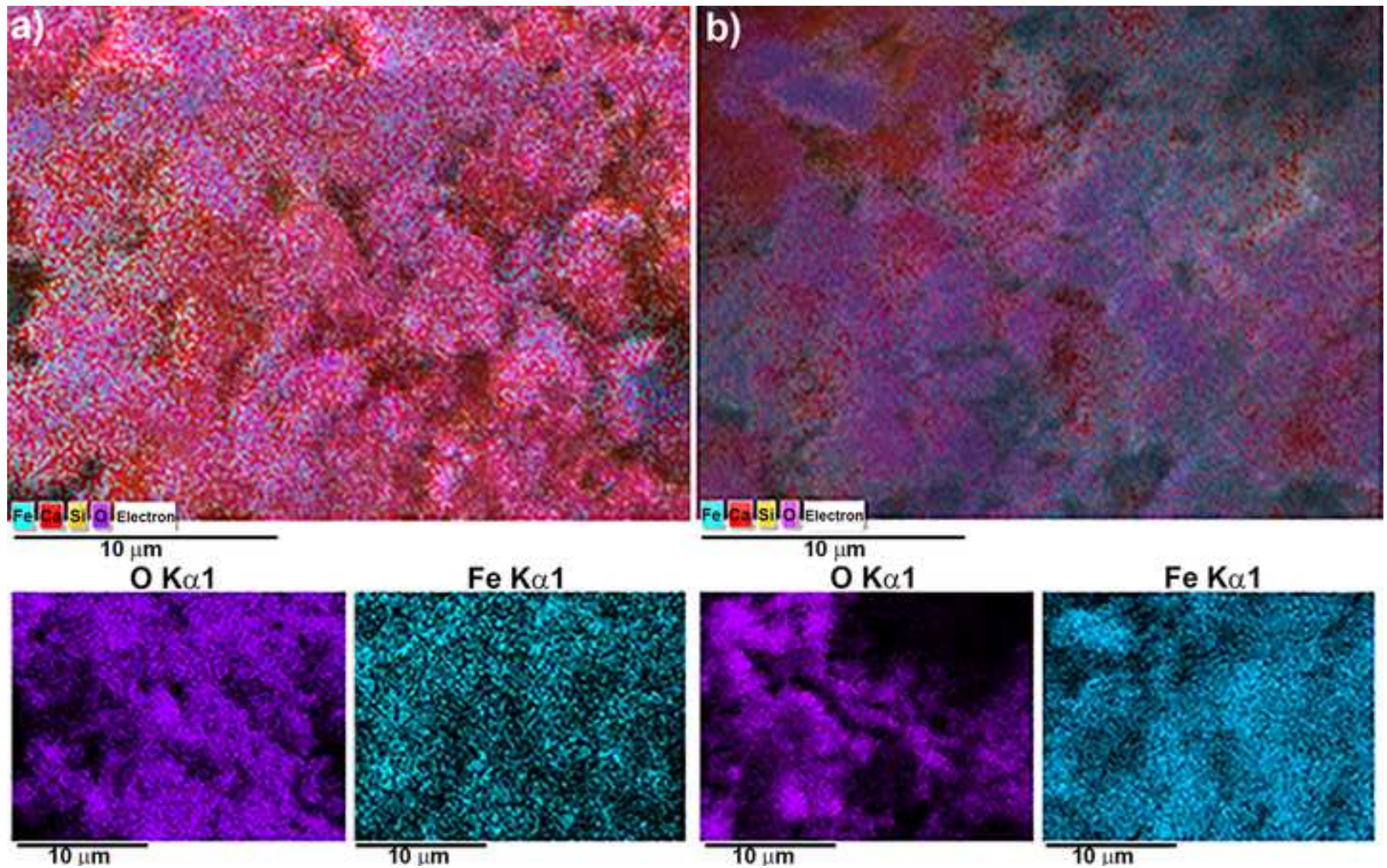


Figure7

[Click here to access/download;Figure;Fig 7.jpg](#)







Ref.: Ms. No. ESPR-D-18-08952R1

Controllable Synthesis of Fe_3O_4 -Wollastonite Adsorbents for Efficient Heavy Metal Ions/Oxyanions Removal Environmental Science and Pollution Research

Reviewers' comments:

Reviewer #1: The authors have tried their level best to address the issues raised by the reviewers. They have modified the manuscript extensively incorporating all the reviewer's suggestions. So the reviewer accepts the revised manuscript and recommends for its possible publication in the Journal of Environmental Science and Pollution Research.

Answer: Authors are very grateful for the reviewers' recommendation.

Reviewer #2: Dear editor and authors,

The paper was improved, but this version is not adequate for publication for these reasons:

1. Please review the English Language in the last part of the paper.

Answer: According to the reviewer advice, the last part of the Manuscript is grammar and spell checked by recommended English speaker.

2 The calculation of adsorption energy through statistical physics model is not correct. Please check the references. Thank you

Answer: According to the reviewer advice, the new method is used for the calculation of adsorption energy. Adsorption energy is calculated according to the following equation

$$\varepsilon = k_B T \ln \left(\frac{c_s}{c_{1/2}} \right), \text{ presented in the recommended literature references (Sellaoui et al., Phys.}$$

Chem. Chem. Phys. 2017,19, 25927-25937 and Sellaoui et al., Env-Sci and Pollution Research, 2017, 24,19902–19908). The corrected values of the adsorption energy and of the corresponding parameters (density of receptor site and number of ions that interact with one receptor site) are presented in Table 5.

Reviewer #3: -